SC-CR-66-2010

B4

AEROSPACE NUCLEAR SAFETY

SC-CR-66-2010

December 1965

PARTICLE FALLOUT AND DISPERSION IN THE ATMOSPHERE QUARTERLY REPORT NO. 2 1 SEPT TO 30 NOV 1965 (U)

Prepared by
K. D. Hage and P. S. Brown
The Travelers Research Center, Inc.
250 Constitution Plaza
Hartford, Connecticut

20000912 084

SANDIA CORPORATION

PRIME CONTRACTOR TO THE U.S. ATOMIC ENERGY COMMISSION | ALBUQUERQUE, NEW MEXICO; LIVERMORE, CALIFORNIA; TONOPAH, NEVADA

DTIC QUALITY INSPECTED 4

Reproduced From
Best Available Copy

Lovelace Foundation - Document Library
22528 NOV 21 1966

Issued by
Sandia Corporation,
a prime contractor to the
United States Atomic Energy Commission

LEGAL NOTICE

This report was prepared as an account of Government sponsored work. Neither the United States, nor the Commission, nor any person acting on behalf of the Commission:

A. Makes any warranty or representation, expressed or implied, with respect to the accuracy, completeness, or usefulness of the information contained in this report, or that the use of any information, apparatus, method, or process disclosed in this report may not infringe privately owned rights; or

B. Assumes any liabilities with respect to the use of, or for damages resulting from the use of any information, apparatus, method, or process disclosed in this report.

As used in the above, "person acting on behalf of the Commission" includes any employee or contractor of the Commission, or employee of such contractor, to the extent that such employee or contractor of the Commission, or employee of such contractor prepares, disseminates, or provides access to, any information pursuant to his employment or contract with the Commission, or his employment with such contractor.

Printed in USA. Price ~~$3.00~~. Available from the Clearinghouse for Federal Scientific and Technical Information, National Bureau of Standards
U. S. Department of Commerce, Springfield, Virginia 22151

SC-CR-66-2010

PARTICLE FALLOUT AND DISPERSION IN THE ATMOSPHERE
QUARTERLY REPORT NO. 2
1 SEPT TO 30 NOV 1965 (U)

Prepared by
K. D. Hage and P. S. Brown
The Travelers Research Center, Inc.
250 Constitution Plaza
Hartford, Connecticut

for

Sandia Corporation
under
Contract No. 48-2417

December 1965

ABSTRACT

Progress is described on the development of an atmospheric fallout model to be used to estimate particulate concentrations in the air and on the earth's surface for particles released at any altitude up to 90 km. The particle size range of interest for this study is 1 to 200 microns in diameter. The model is being programed to be run on a CDC 3600 computer. During this quarter, preliminary specifications and coding for the program were completed for all but one major component of the model.

SUMMARY

Knowledge of the fate of radioactive fuel particles injected into the atmosphere by a re-entering SNAP device is necessary in order to determine if any hazard could exist to the general population. It is the purpose of the work under this contract to develop a theoretical atmospheric model, programmed to be run on a CDC 3600 computer, that can be used to predict the fallout pattern and ultimate ground concentrations of particulates in the size range of 1 to 200 microns released as a line source anywhere in the atmosphere up to altitudes of 90 km.

In this report, data is given on the preliminary computer program specifications developed for the fallout model. Details on the development and coding of computer program specifications for such items as particle fall speeds, mass-element trajectories, as well as the methods for representing zonal flow and long atmospheric waves are presented.

TABLE OF CONTENTS

LIST OF ILLUSTRATIONS

LIST OF TABLES

LIST OF TABLES

PARTICLE FALLOUT AND DISPERSION IN THE ATMOSPHERE

1.0 INTRODUCTION

In the first Quarterly Progress Report, issued under Sandia Corporation Contract No. 48-2417, qualitative descriptions were given of the principal components or subroutines of a computer program for the fallout and dispersion of solid particles released from a source in the stratosphere [8]. The mathematical framework for the simulation of large-scale atmospheric flow in the model was also presented.

The present report describes progress during the second quarter (September—November, 1965). Preliminary computer program specifications were completed for the fallout model and coding was completed for all major components except the mass-element expansion and subdivision routine. Special attention was given to the problem of selecting appropriate particle fall-speed equations for the wide range of Reynolds numbers, Knudsen numbers, and Mach numbers that must be considered for particles from ten to several hundred microns in size falling from altitudes up to 90 km. The transient acceleration phase of fall was investigated for particles with both small and large initial fall speeds.

Two methods of numerical integration of particle trajectories were programmed and tested using simulated equations of motion which possess some of the characteristics expected in more realistic trajectories, and yet are of sufficiently elementary forms so that exact solutions could be obtained for test purposes. The trajectory computations are one of the most critical parts of the model and further testing is planned for the third quarter.

Several computer programs required for fitting the mathematical functions described in [8] to observed or analyzed winds were prepared and checked. Fitting of meridional profiles of the east—west or zonal mean winds at ten levels (summer and winter seasons) and the large-scale eddy flow at two levels (winter season) was completed. Vertical fitting of the mean zonal flow was near completion at the end of the quarter. Available sources of data that can be used readily for this purpose have apparently been exhausted and further progress will require specification based on known properties of the flow and additional harmonic analyses of wind or pressure observations.

2.0 PARTICLE FALLOUT AND DISPERSION MODEL (Model B)

2.1 Source Description

Because Model B does not take into account the processes of particle formation, it is necessary to select one instant in time during reentry that can be used to specify the required initial conditions for the model. In general, the elapsed time between particle formation and the moment for which initial conditions are specified should be small enough so that cloud growth by gravitational sorting and by turbulent dispersion is small, but large enough so that their velocities are essentially independent of particle velocities at the time of formation. The latter requirement is examined in some detail in Section 2.2.4.

At the initial moment (t = 0 in Model B) it is assumed that the particle cloud has the form of a simple line or arc segment with a circular cross-section and finite length roughly analagous to a meteor trail or a high-altitude aircraft contrail. In the model, this source cloud is simulated by one to twenty discrete elements. Each element takes the form of a trivariate normal distribution of particles in space characterized by the following parameters:

(a) Position (altitude, latitude, and longitude)

(b) Dimensions (standard deviations of the particle distribution in the meridional, zonal, and vertical directions)

(c) Source Strength (total mass of particles)

(d) Mass-Diameter Distribution

In this report, reference will be made only to a single source element, because the final concentration field and deposit patterns for the total particle cloud are obtained by simple superposition and smoothing of contributions from all source elements. In other words, the transport and growth of an individual source cloud element is treated independently of all other elements.

As indicated by (d) above, each source cloud element is characterized by a particle-size distribution. In the model the particle size distribution is divided into discrete mass elements, each containing a fixed equal fraction of the total mass in the form of particles of uniform size. Three options are available for specifying the mass-diameter distribution; a log-normal distribution characterized by mass-median

diameter δ_m and logarithmic standard deviation ν; a discrete distribution characterized by mass-median diameters for each mass element, and; an unspecified distribution function other than the log-normal that may be added to the program if desired. Each source element can be subdivided into 1, 20, 50, or 100 mass elements. The first of these corresponds to a monodisperse particle population. The source description subroutine of the computer program for Model B has been coded and verified.

2.2 Particle Fall Speeds

2.2.1 Atmospheric Parameters

In Model A, the terminal velocities of the particles contained in each mass element were required only at preselected altitudes; consequently, the numerical values of air density, viscosity, and mean free path were required only at these altitudes. In Model B, however, the altitudes at which these variables are required are determined during the trajectory integrations. In general, these altitudes will be unequally spaced and will vary from one mass element to another. For purposes of interpolation, the following polynomials were obtained by least-squares fitting procedures using 1962 U.S. standard atmosphere values of air density [ρ (gm cm^{-3})], viscosity [(μ(gm cm^{-1} sec^{-1})], and mean free path [λ(cm)] tabulated at 1.0 km height intervals from 0.5 km to 89.5 km [4].

$$\rho = \exp \{ - 6.697 - 8.992 \times 10^{-2} z - 2.510 \times 10^{-3} z^2 + 1.206 \times 10^{-5} z^3 + 7.748 \times 10^{-7} z^4 - 8.199 \times 10^{-9} z^5 - 2.519 \times 10^{-11} z^6 + 3.703 \times 10^{-13} z^7 \} \quad (2\text{-}1)$$

$$\mu = 1.802 \times 10^{-4} - 4.362 \times 10^{-6} z + 1.173 \times 10^{-7} z^2 + 8.877 \times 10^{-10} z^3 - 4.715 \times 10^{-11} z^4 + 3.107 \times 10^{-13} z^5 \quad (2\text{-}2)$$

$$\lambda = 8.125 \times 10^{-5} \rho^{-1}. \quad (2\text{-}3)$$

The root-mean-square (rms) error, the mean absolute error, and the extreme errors were all considered in the selection of these polynomials. These quantities are shown in Table 2-1 for polynomials of various degrees.

TABLE 2-1
ERROR SUMMARY FOR POLYNOMIAL REPRESENTATION OF STANDARD ATMOSPHERE VALUES OF DENSITY AND VISCOSITY TO 90 km

Parameter	Degree of polynomial	Rms error ($\times 10^{-6}$)	Mean absolute error (%)	Extreme error (%)	
				Minimum	Maximum
Density	4	5.2	1.67	-4.3	+9.3
	7	4.2	1.02	-2.4	+4.2
	8	3.9	0.96	-2.4	+4.2
	9	3.6	1.02	-2.2	+3.9
Viscosity	3	7.6	4.43	-9.1	+18.1
	5	1.4	0.76	-2.8	+1.5
	7	1.4	0.76	-2.9	+1.6
	9	1.4	0.74	-3.0	+1.6

Because the errors associated with a seventh-degree polynomial for density and a fifth-degree polynomial for viscosity are of the same order of magnitude as departures from standard atmosphere values caused by daily changes in atmospheric structure, and because little reduction in error can be realized without a large increase in degree, the seventh- and fifth-degree equations were selected. The percent errors at each data point from the surface to 89.5 km are shown in Fig. 2-1 for density and viscosity. In both cases, the largest error occurred at the tropopause level (near 10 km) in the standard atmosphere. The error profile for mean free path is a mirror image of that for density. Greater accuracy can be achieved with lower order polynomials if the total layer is subdivided into smaller layers. However, this is not acceptable in the present problem because serious errors may be introduced in the trajectory computations due to discontinuities in the time derivatives of particle fall speed.

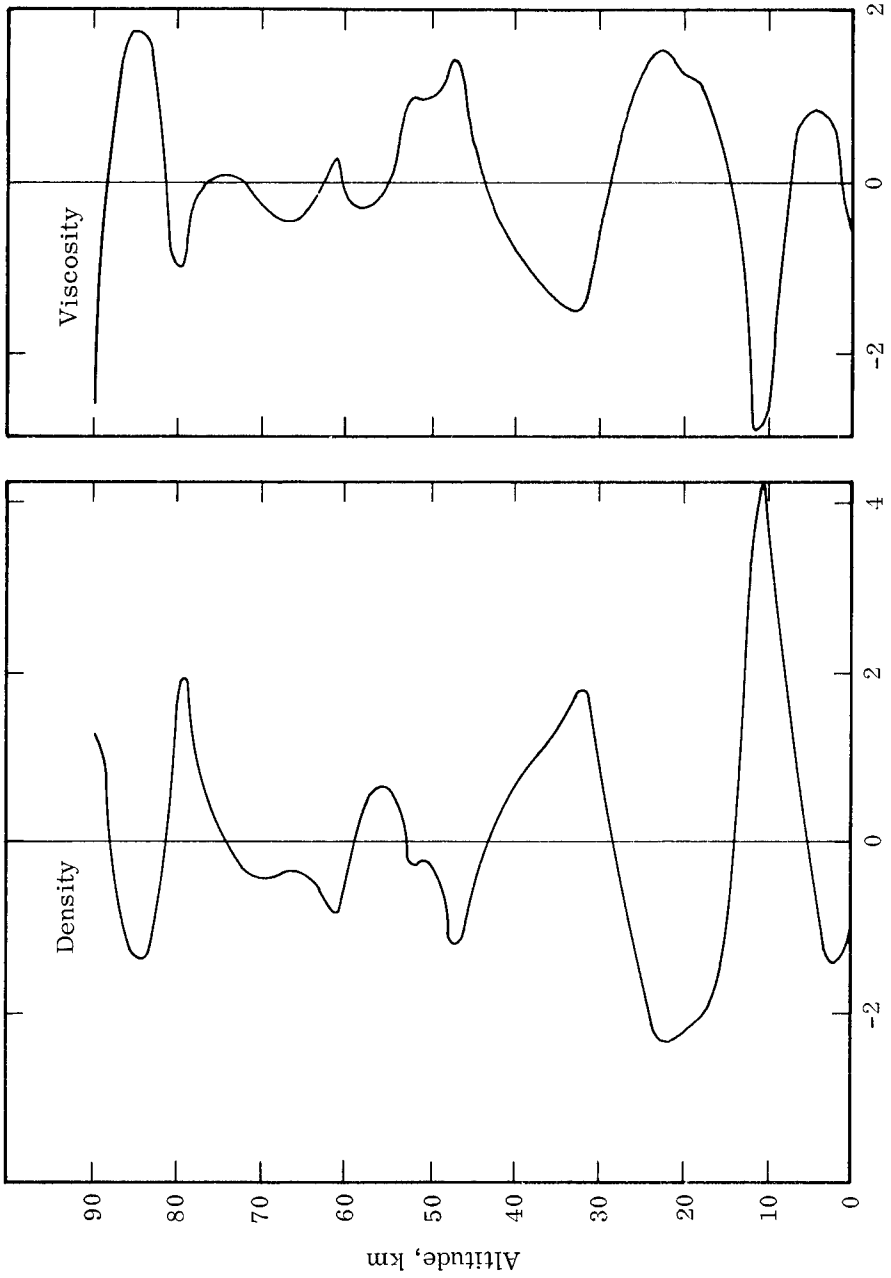

Fig. 2-1. Vertical profiles of errors (%) associated with polynomial representation of U.S. standard atmosphere densities and viscosities.

At the user's option, alternative tabulations of density and viscosity not too different from the U.S. standard atmosphere values can be used in the model. If this option is used, new coefficients are computed for Eqs. (2-1), (2-2), and (2-3) by a least squares fit to the desired values.

2.2.2 Drag-force Equations

The resistance or drag force acting on a particle moving steadily through the atmosphere depends on the Reynolds number, $R_e = \frac{W\rho d}{\eta}$; a particle shape factor $B = \frac{Sd}{2V}$; the Knudsen number $K_n = \lambda/d$; and; the Mach number $M = W/v_s$. In these expressions, W is the particle speed, ρ is air density, d is particle diameter, η is air viscosity, S is the particle cross-sectional area, V its volume, λ the mean free path, and v_s the speed of sound. For solid spheres, the shape factor B has a minimum numerical value of 3. Following Öpik [14] and Davies [3], the drag force F can be formulated as follows for various ranges of the nondimensional parameters:

$$F_1 = \frac{\pi d^2}{4} \rho(W^2 + 1.5u^2) \qquad (M > 1;\ K_n > 1) \qquad (2\text{-}4)$$

$$F_2 = \frac{\chi\pi d^2}{4} \rho W^2 \qquad (M > 1;\ K_n \leq 1;\ F_2 > F_3) \qquad (2\text{-}5)$$

$$F_3 = \frac{\chi\pi}{8\rho} \eta^2 R_e^2 \qquad (M > 1;\ K_n \leq 1;\ F_2 \leq F_3) \qquad (2\text{-}6)$$

$$F_4 = \frac{2.5\pi}{4} d^2 \rho\mu W \qquad (M \leq 1;\ K_n > 1;\ F_4 > F_2) \qquad (2\text{-}7)$$

$$F_2 = \frac{\chi\pi}{8} d^2 \rho W^2 \qquad (M \leq 1;\ K_n > 1;\ F_4 \leq F_2) \qquad (2\text{-}8)$$

$$F_3 = \frac{\chi\pi}{8\rho} \eta^2 R_e^2 \qquad (M \leq 1;\ K_n \leq 1;\ F_3 > F_2) \qquad (2\text{-}9)$$

$$F_2 = \frac{\chi\pi}{8} d^2 \rho W^2 \qquad (M \leq 1;\ K_n \leq 1;\ F_3 \leq F_2). \qquad (2\text{-}10)$$

In the formula for F_1, the quantity u is the root-mean-square thermal velocity component along one coordinate ($u = [kT/m]^{1/2}$) where k is the Boltzman constant, T is temperature, and m is the mass of one mole of air. The parameter χ in the formula for F_2 is the drag coefficient. Values of χ recommended by Öpik [14] are given in Table 2-2.

TABLE 2-2
DRAG COEFFICIENT FOR SHIELDED HIGH-SPEED FLOW [14]

$0.75/K_n$	Mach number (M)	Drag coefficient (χ)
0	$M \gg 1$	2.00
1	$M \gg 1$	1.50
2	$M \gg 1$	1.25
4	$M \gg 1$	1.12
∞	$M \gg 1$	1.00
∞	$M \leq 1$	0.50

Values of χ required in the formula for F_3 are implicit in Davies interpolation equations for R_e [3].

$$R_e = \frac{\chi Re}{2\ 4}^2 - 2.3363 \times 10^{-4} (\chi R_e^{2})^2 + 2.0154 \times 10^{-6} (\chi R_e^{2})^3 - 6.9105 \times 10^{-9} (\chi R_e^{2})^4 \qquad (R_e < 4) \tag{2-11}$$

$$\log R_e = -1.29536 + 0.986 (\log \chi R_e^{2}) - 4.6677 \times 10^{-2} (\log \chi R_e^{2})^2 + 1.1235 \times 10^{-3} (\log \chi R_e^{2})^3 \qquad (3 < R_e < 10^4) \tag{2-12}$$

The drag coefficients given by Eqs. (2-11) and (2-12) are used when the viscosity of the air is important, while those in Table 1 are for high-speed, low-density flow. When the Knudsen number is near unity, Eqs. (2-6) and (2-9) can be used only if the Reynolds number is small, because the slip flow corrections for these equations are not known for large Reynolds numbers. Experimental measurements of the drag coefficients of spheres moving at high speed in a low-density medium are being sought in an attempt to check the theoretical values in Table 2-2.

2.2.3 Terminal Velocities

A falling particle reaches its terminal velocity in the atmosphere when the drag force equals the attractive force of gravity. For a sphere of large density in air,

$$F = \frac{\pi}{6} d^3 \rho_p g \tag{2-13}$$

where ρ_p is the particle density and g is the acceleration of gravity. The terminal velocity $W = W_T$ may be derived from Eq. (2-13) using Eqs. (2-4) to (2-12) for F. Computations of W_T have been made for selected particle sizes in atmospheric layers for which the Mach number and Knudsen number are near unity, i.e., in regions of the atmosphere for which formulas F_1, F_2, F_3, and F_4 overlap. Terminal velocities according to Eqs. (2-4), (2-7), and (2-11) for a 500 micron diameter sphere (density 5) falling between 60 and 90 km under standard atmosphere conditions are shown in Fig. 2-2. For this particle size and altitude range, the Reynolds number is less than one, the mean free path exceeds the particle size above about 59 km, and the Mach number exceeds one above about 72 km. Equation (2-11) yields the largest drag force up to about 78 km, because Eq. (2-7) is invalid below 59 km. Above 78 km, Eq. (2-4) for unshielded supersonic flow is more appropriate than Eq. (2-11). It is clear from the divergence of the curves above 78 km in Fig. 2-2 that there exists a region for large particles and high altitudes in which the terminal velocity equations used in fallout Model A [Eqs. (2-11) and (2-12)] are invalid. Two other regions in which these equations are invalid have been identified. The first of these first appears at altitudes of about 40 km as particle size is increased and is associated with the conditions $R_e > 1$, $K_n > 1$. The second of these regions occurs at lower altitudes for $R_e > 1$, $K_n < 1$, and Mach numbers of the order of 1 or larger. The validity of Eqs. (2-5), (2-6), (2-8), (2-9), and (2-10) for the computation of terminal velocity in these regions is under study.

The behavior of terminal velocities computed from Eqs. (2-7) and (2-11) for a smaller particle of 11 microns diameter (density 5) is shown in Fig. 2-3. In this case $R_e \ll 1$ and $K_n = 1$ at about 33 km. Equation (2-11) is selected here because it yields the greatest drag force at all altitudes between 33 and 90 km. The curves above 70 km (not shown in Fig. 2-3) are nearly parallel.

2.2.4 Particle Acceleration

Although the transient acceleration phase experienced by a particle with an initial velocity different from its terminal velocity is negligible, in the lowest layers of the atmosphere, for most particles of interest in the present problem, it is significant at high altitudes. The drag forces for two limiting cases of high altitude flow

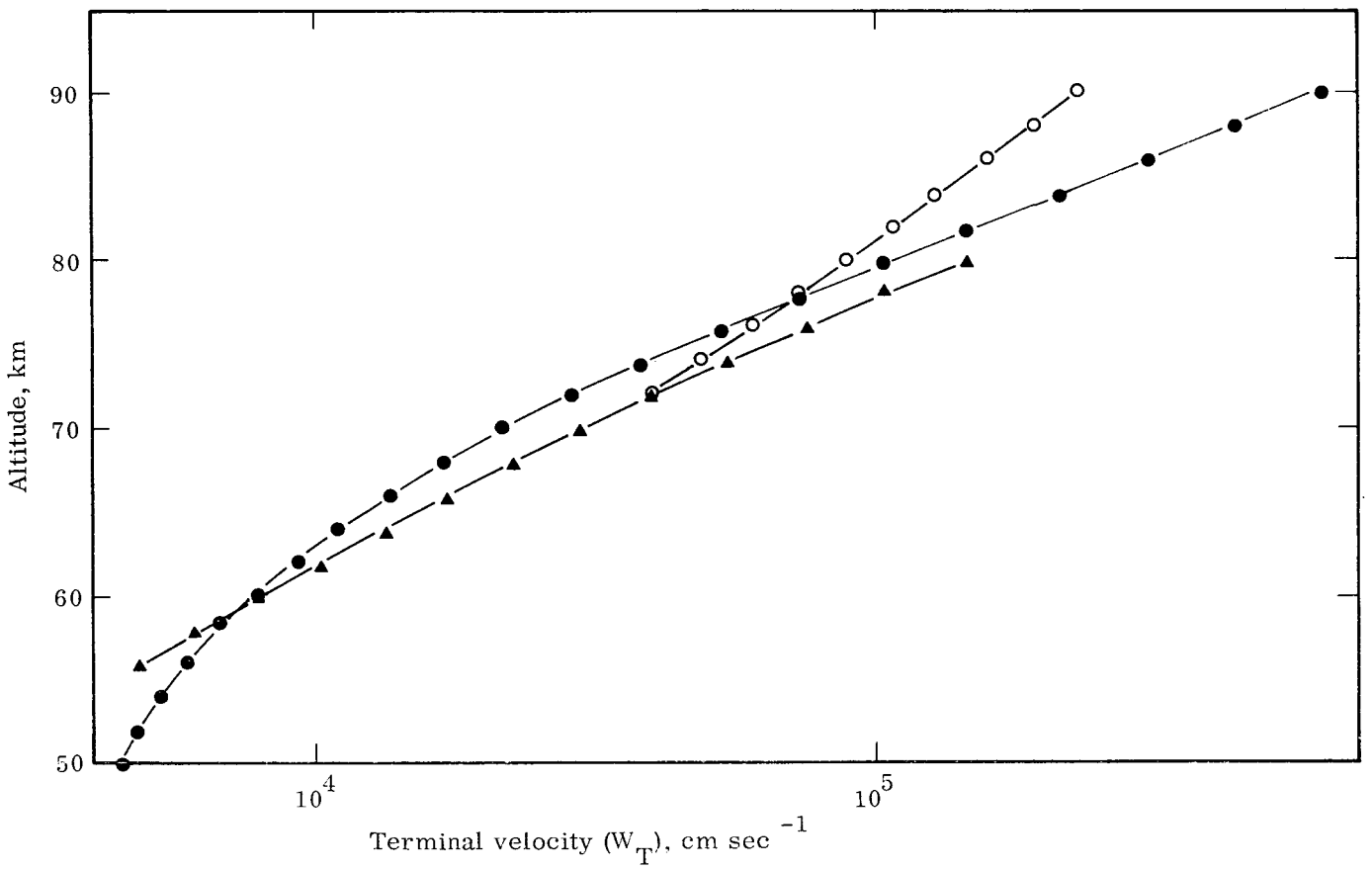

Fig. 2-2. Terminal velocities based on drag force formulation for shielded viscous flow [●, Eq (2-11)], unshielded subsonic flow [▲, Eq (2-7)], and unshielded supersonic flow [○, Eq (2-4)] for a 500-micron diameter sphere (density 5).

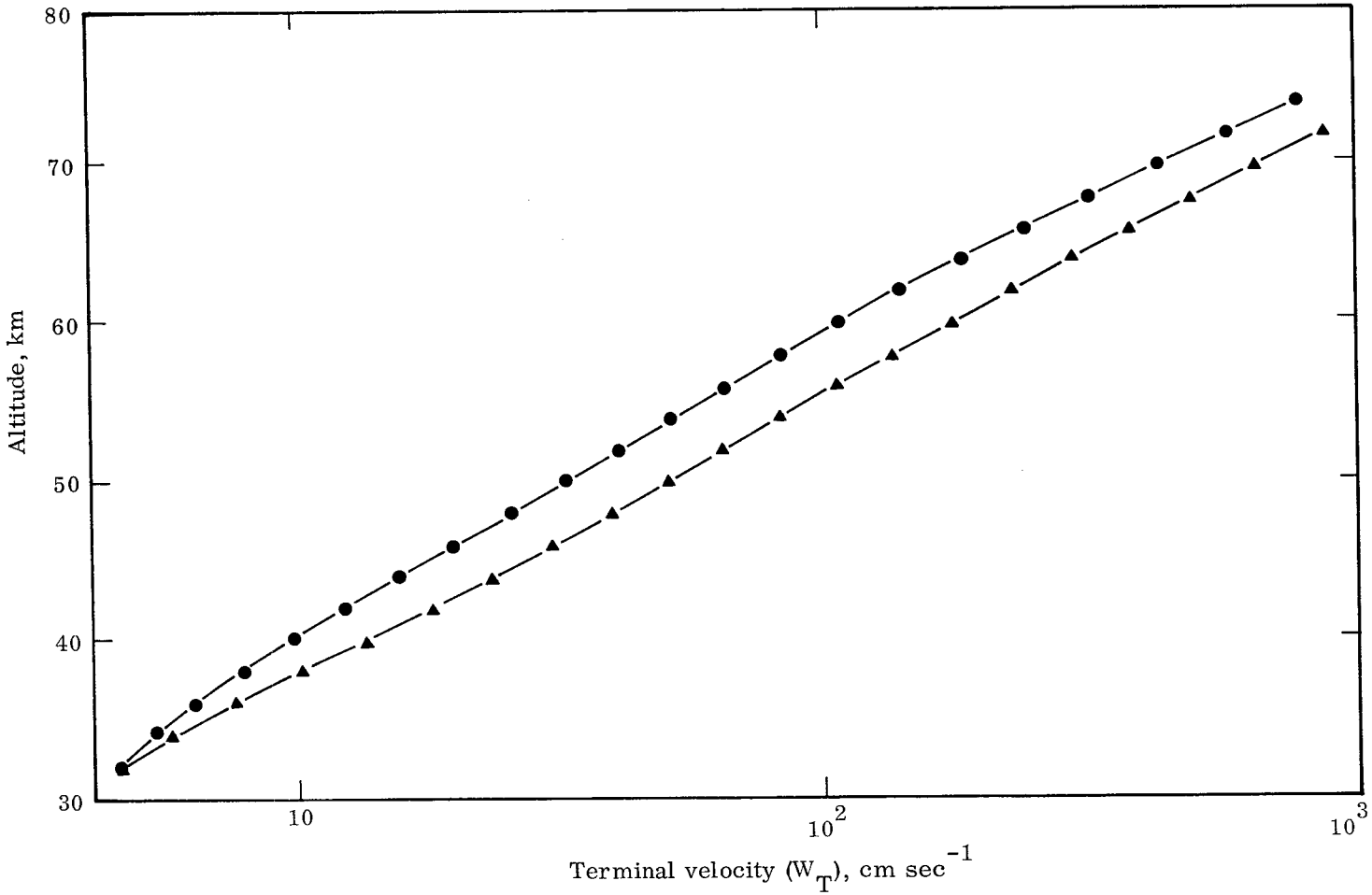

Fig. 2-3. Terminal velocities based on drag force formulations for viscous slip flow [●, Eq (2-11)] and unshielded subsonic flow [▲, Eq (2-7)] for a 11-micron diameter sphere (density 5).

are given by Eq. (2-4) (large W) and Eq. (2-7) (small W). In the latter case, the resistance force is proportional to W and the particle acceleration is given by

$$\frac{dW}{dt} = g - \frac{k_1 W}{m} \tag{2-14}$$

where m is the particle mass and k_1 is a constant. Assuming constant atmospheric parameters, this may be integrated to give

$$W = W_T \{1 - [1 - W_0/W_T] \exp - (g^{t/W_T})\} \tag{2-15}$$

where $W = W_0$ at $t = 0$. If the particle falls from rest, the characteristic time or time constant of the acceleration phase is W_T/g. However, with a non-zero initial velocity, W_0 the characteristic time for the acceleration phase depends also on the ratio W_0/W_T. Solving for t in Eq. (2-15), we find

$$t = W_T/g \ \ln \left\{ \frac{(1 - W_0/W_T)}{(1 - W/W_T)} \right\}. \tag{2-16}$$

The times t required to reach fall speeds W within 10 percent of the particle terminal velocity W_T are shown in Fig. 2-4 for two extreme initial velocities ($W_0 = 0$ and $W_0 = 18{,}000$ mph).

According to Eq. (2-4) for large values of W (i.e., $W > u$), the resistance force is proportional to W^2 and the particle acceleration is given by

$$\frac{dW}{dt} = g - \frac{k_2 W^2}{m} . \tag{2-17}$$

Again assuming constant atmospheric parameters, Eq. (2-17) yields, after integration:

$$W = W_T \ (\exp \ 2gt/W_T + 1)^{-1} \left\{ \left(\frac{W_T + W_0}{W_T - W_0} \right) \ \exp (2gt/W_T) - 1 \right\} \tag{2-18}$$

where $W = W_0$ at $t = 0$ ($W_0 \neq W_T$). Solving for t in Eq. (2-18) gives

$$t = \frac{W_T}{2g} \ \ln \left\{ \frac{(1 + W_0/W_T)\ (1 - W_0/W_T)}{(1 - W/W_T)\ (1 + W_0/W_T)} \right\} . \tag{2-19}$$

The times t required to reach fall speeds W within 10 percent of the particle terminal velocity W_T are shown in Fig. 2-5 for the same initial velocities as those

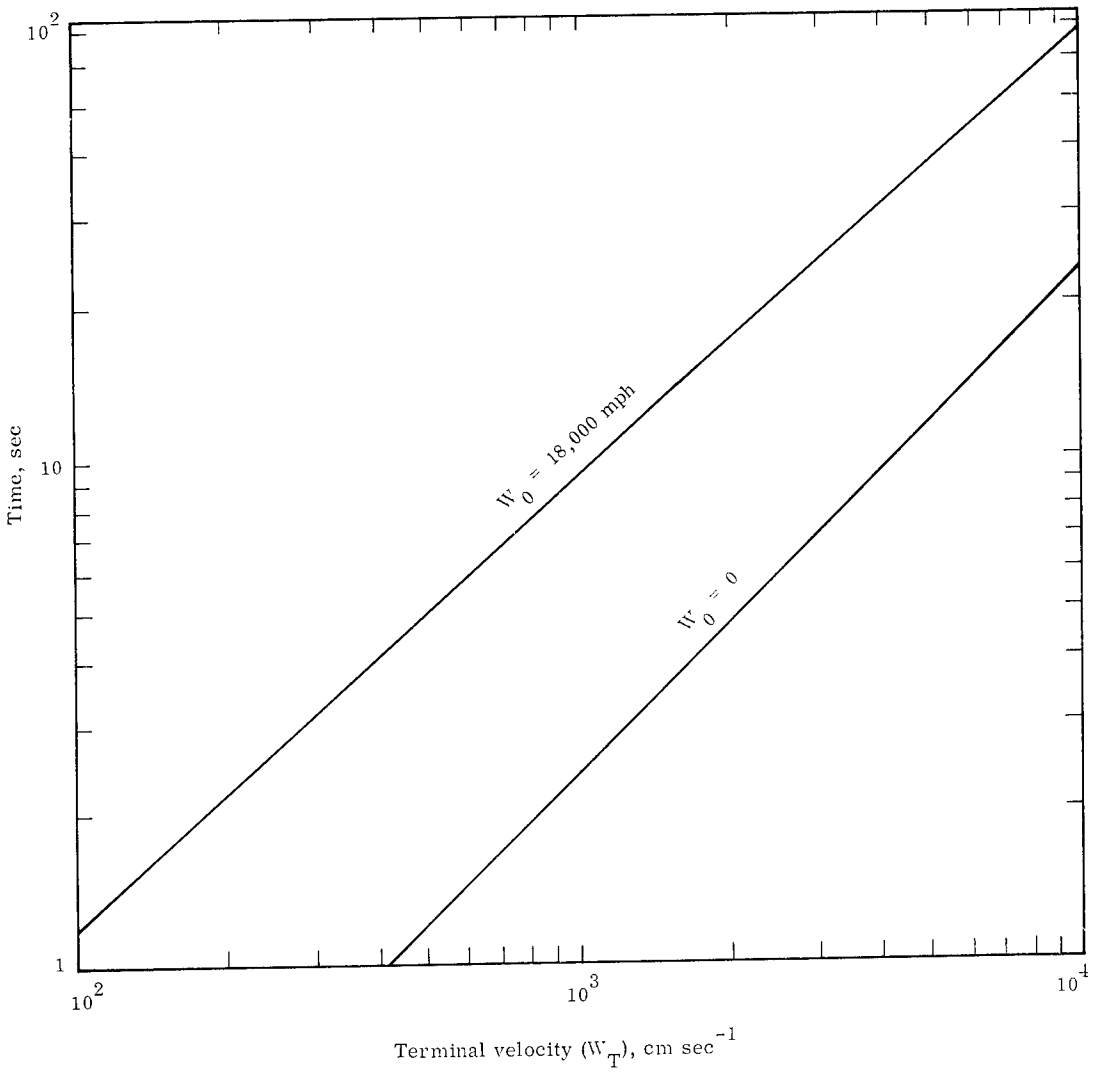

Fig. 2-4. Time required to attain fall speed within 10 percent of terminal velocity for two extreme initial velocities W_0 with drag force proportional to particle speed.

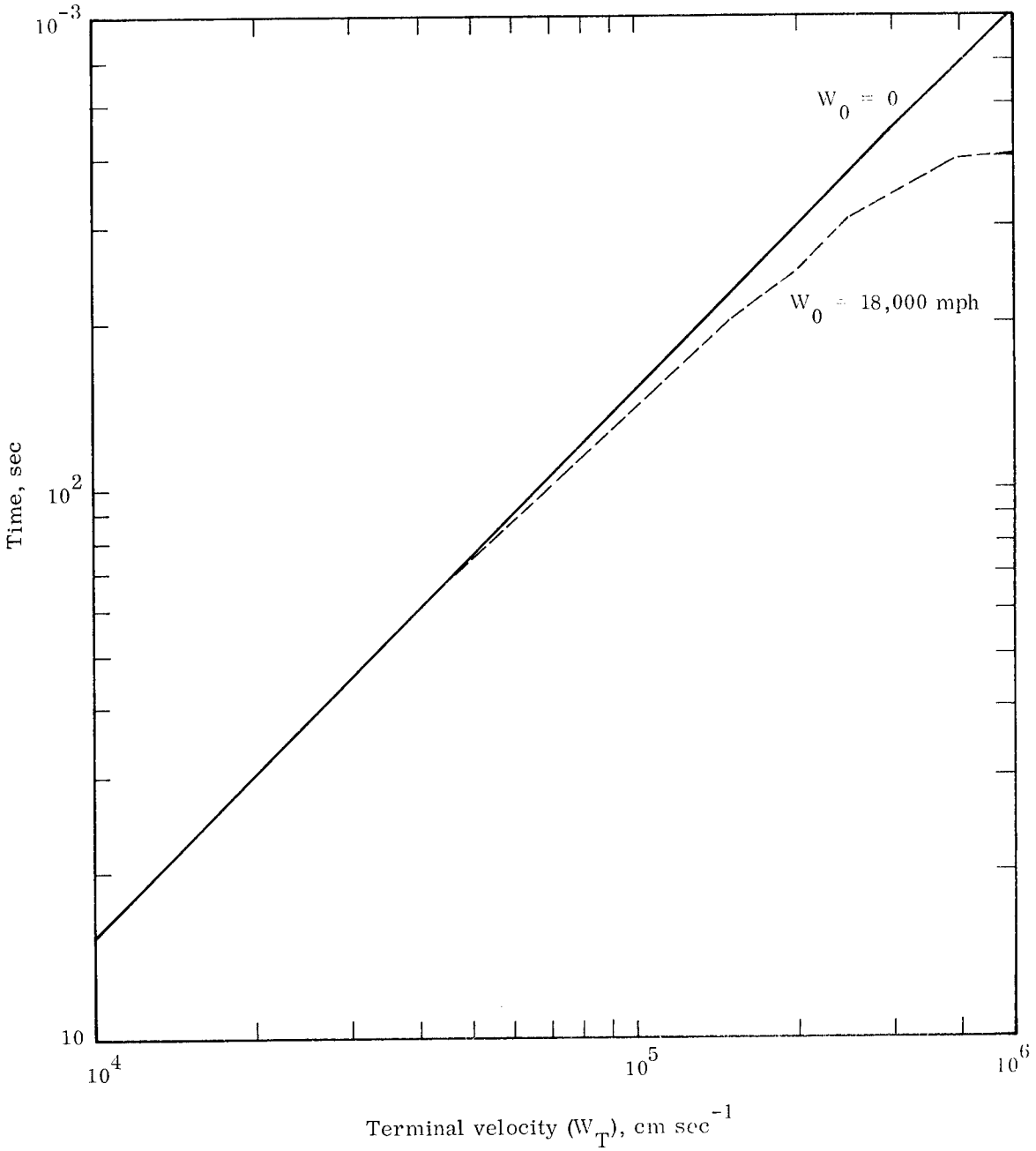

Fig. 2-5. Time required to attain fall speed within 10 percent of terminal velocity for two extreme initial velocities W_0 with drag force proportional to the square of particle speed.

used in Fig. 2-4.

Because terminal velocities in excess of 10^3 cm sec^{-1} are found even for particles of the order of 10 microns diameter at the highest altitudes of interest, it is apparent from Figs. 2-4 and 2-5 that rather severe limitations must be placed either on particle size or altitude unless the acceleration phase is taken into account.

Although the characteristic times in Figs. 2-4 and 2-5 indicate that particle accelerations are important, these accelerations cannot be used to estimate the effect of acceleration on particle residence time because, due to changes in air density, viscosity, and mean free path, the particle terminal velocities decrease rapidly with a decrease in altitude. Numerical integrations of the fall-speed equations, which take into account both the accelerations and the changes in drag forces with altitude, have been undertaken in an effort to identify the upper limits of particle size and altitude for which accelerations may be neglected in terms of effect on total residence time or net horizontal displacement in deep layers. In the reentry fallout problem, the particle accelerations may be of importance only if they lead to appreciable changes in the time of arrival or position of particles at levels of 10 km or lower.

2.3 Mass-element Trajectories

2.3.1 Introduction

The positions of the mass elements or subdivisions of each particle source-cloud element must be known at specified levels in the atmosphere to compute air concentrations and deposit densities at the earths' surface. The equations for the position of the center of a mass-element at the (r + 1) time step are:

$$\theta_{r+1} = \theta_r + \int_{t_r}^{t_{r+1}} \dot{\theta}(\theta, \lambda, z, t)\, dt \tag{2-20}$$

$$\lambda_{r+1} = \lambda_r + \int_{t_r}^{t_{r+1}} \dot{\lambda}(\theta, \lambda, z, t)\, dt \tag{2-21}$$

$$z_{r+1} = z_r + \int_{t_r}^{t_{r+1}} \{ W(z) + w(\theta, \lambda, z, t) \} dt \tag{2-22}$$

where θ (colatitude), λ (longitude), and z (altitude) are position coordinates in the atmosphere, t is time, W(z) is the terminal velocity of particles in a mass-element,

$\dot{\theta}$ and $\dot{\lambda}$ are the meridional and zonal components, respectively, of the angular velocity of the air, and w is the vertical air velocity. It is assumed that the horizontal particle velocity is equal at all times to the local horizontal air velocity and that the vertical particle velocity is equal to the sum of the particle terminal velocity and the local vertical air velocity. The latter assumption was discussed in Section 2.2.4.

Because of the complexity of the analytic forms for $\dot{\theta}$, $\dot{\lambda}$, W, and w, it is necessary to evaluate Eqs. (2-21), (2-22), and (2-23) by numerical methods. Numerous methods of integration are available and it becomes a matter of selecting the optimum one for this problem.

The principal selection criteria are:

(a) The position of the end-point of the trajectory must be insensitive to such details of the method of computation as the choice of time-step length, the choice of criteria for the control of individual time step errors, etc.

(b) It should be possible to estimate reliably and with ease the initial time-step length and subsequent changes in time-step length as required to achieve (a).

(c) The computation time should be minimized.

(d) The programming and verifying procedures should be as straightforward and simple as possible, consistent with (a), (b), and (c).

The accuracy requirements described by (a) above can be determined quantitatively by comparing the accumulated position errors with estimates of uncertainty due to natural diffusion processes. If the particle position errors due to computation are large, an artificial particle-cloud growth rate will result and the estimates of concentrations and deposit densities will be meaningless.

Two specific methods of integration representing the one-step Runge–Kutta method and the multi-step predictor–corrector class of methods were selected for testing. Both methods were programmed, checked, and subjected to preliminary performance tests on simplified equations possessing some of the properties of the equations that will later be used to simulate the atmospheric wind field. This work is described in more detail in the following sections.

2.3.2 Runge—Kutta Integration Method

Equation (2-22) for particle height will be used to illustrate the Runge—Kutta procedure. If h is the time step,

$$z(t_0 + h) = z(t_0) + \int_{t_0}^{t_0\ th} W[t, z(t)]\ dt \tag{2-23}$$

omitting the term w (θ, λ, z, t) for simplicity. The Runge–Kutta formulas represent an approximation (to a specified order of accuracy) to a formal Taylor's series expansion for $z(t_0 + h)$. The approximation requires the evaluation of first derivatives only. The following quantities are needed for a fourth order approximation, i.e., exact agreement with a Taylor series expansion through terms of order h^4:

$$\begin{aligned}
a_1 &= h\,W(t_0, z_0) \\
a_2 &= h\,W(t_0 + b, h, z_0 + c_1 a_1) \\
a_3 &= h\,W(t_0 + b_2 h, z_0 + c_2 a_1 + d_1 a_2) \\
a_4 &= h\,W(t_0 + b_3 h, z_0 + c_3 a_1 + d_2 a_2 + e_1 a_3)
\end{aligned} \tag{2-24}$$

$$Z(t_0 + h) - Z_0 = f_1 a_1 + f_2 a_2 + f_3 a_3 + f_4 a_4. \tag{2-25}$$

The form of Eqs. (2-24) and (2-25) represents a generalization of the form that results from the approximation of a Taylor's series solution by Simpson's rule. The symbol Z indicates that this quantity is an approximation to $z(t_0 + h)$.

All but one of the parameters b, c, d, e, and f are needed to meet the requirement

$$Z(t_0 + h) = Z(t_0 + h) + 0(h^4).$$

Gill [8], in optimizing the method for use on a computer, chose the arbitrary condition to be $e_1 = 1 + \sqrt{1/2}$. The other parameters are then

$$\begin{aligned}
b_1 &= 1/2 & d_1 &= 1 - \sqrt{1/2} \\
b_2 &= 1/2 & d_2 &= -\sqrt{1/2} \\
b_3 &= 1 & f_1 &= 1/6 \\
c_1 &= 1/2 & f_2 &= 1/3\ (1 - \sqrt{1/2})
\end{aligned}$$

$$c_2 = -1/2 + \sqrt{1/2} \qquad f_3 = 1/3\ (1 + \sqrt{1/2})$$
$$c_3 = 0 \qquad f_4 = 1/6$$

The form of the Runge—Kutta—Gill equations used in the computer program involves auxiliary quantities, g, as recommended by Gill [8] for greater efficiency and round-off error control. The solution is

$$z_4 = z_3 + 1/6\ (a_4 - 2g_3) = Z(t_0 + h) \tag{2-26}$$

where

$$a_1 = h\,W(t_0, z_0) \qquad z_1 = z_0 + 1/2\,(a_1 - 2g_0)$$
$$a_2 = h\,W(z_0 + h/2, z_1) \qquad z_2 = z_1 + (1 - \sqrt{1/2})\,(a_2 - g_1)$$
$$a_3 = h\,W(z_0 + h/2, z_2) \qquad z_3 = z_2 + (1 + \sqrt{1/2})\,(a_3 - g_2)$$
$$a_4 = h\,W(z_0 + h, z_3)$$

(2-27)

$$g_1 = g_0 + 3\,[1/2\,(a_1 - 2g_0)] - 1/2\,a_1$$
$$g_2 = g_1 + 3\,[(1 - \sqrt{1/2})\,(a_2 - g_1)] - (1 - \sqrt{1/2})\,a_2$$
$$g_3 = g_2 + 3\,[(1 + \sqrt{1/2})\,(a_3 - g_2)] - (1 + \sqrt{1/2})\,a_3$$
$$g_4 = g_3 + 3\,[1/6\,(a_4 - 2g_3)] - 1/2\,a_4$$

with $g_0 = 0$ in the first time step and $g_0 = g_4$ in subsequent time steps.

The Runge—Kutta method described above was coded for a system of three equations (θ, λ, and z) following the procedure described by Ralston and Wilf [15]. The coding for the θ and λ equations was checked using a sample problem for which the solutions were readily available [15, p. 119]. Verification of the coding for the solution of the z equation is described in a later section.

2.3.3 Predictor—Corrector Integration Method

Predictor—corrector techniques for the solution of an ordinary differential equation such as $\frac{dz}{dt} = W(z,t)$ involve the prediction of a value of z at $t = t_0 + h$, the computation of an estimate of $\frac{dz}{dt}$ at $t = t_0 + h$ using the predicted z, and the computation of a corrected approximation to z at $t = t_0 + h$. Hamming's method [10] which is both accurate and stable for many integration problems was coded for testing on the trajectory problem. In this method, the corrector is derived by evaluating the coefficients of a linear combination of $z(t_0)$, $z(t_0 - h)$, $z(t_0 - 2h)$, $\dot{z}(t_0 + h)$, $\dot{z}(t_0)$, and $\dot{z}(t_0 - h)$ from a Taylor's series expansion of $z(t_0 + h)$ under the condition that

all powers of h through h^4 vanish. The accuracy of the predictor is greatly increased by the use of a modifier derived from an estimate of the truncation error at each step. Using the notation p for predictor, m for modifier, and c for corrector, and numerical subscripts to identify the time of evaluation of each term relative to t_0, the integration equations are:

$$\begin{aligned} p_1 &= z_{-3} + \frac{4h}{3}(2\dot{z}_0 - \dot{z}_{-1} + 2\dot{z}_{-2}) \\ m_1 &= p_1 - \frac{112}{121}(p_0 - c_0) \\ \dot{m}_1 &= W(t_1, m_1) \\ c_1 &= \frac{1}{8}\{9z_0 - z_{-2} + 3h(\dot{m}_1 + 2\dot{z}_0 - \dot{z}_{-1})\} \end{aligned} \tag{2-28}$$

$$z_1 = c_1 + \frac{9}{121}(p_1 - c_1) \tag{2-29}$$

The above method has an important advantage over the Runge–Kutta method because it provides an estimate of the error at each step and these estimates can be used to change the step length. However, the method is not self-starting. In the first version that was programmed, the Runge–Kutta method was used exclusively for both starting and changing step length. However, due to the need for frequent changes in step length in test trajectory problems, this approach did not provide a suitable basis for comparing the performance of the two integration techniques. Consequently, a second version using stored values of z for doubling the time step and interpolated values of z for halving the time step was prepared. The interpolation formulas quoted by Ralston and Wilf [15, p. 103] were used because they possess the same order of accuracy as the integration method.

$$\begin{aligned} z - 1/2 &= \frac{1}{256}(80z_0 + 135z_{-1} + 40z_{-2} + Z_{-3}) \\ &\quad + \frac{h}{256}(-15\dot{z}_0 + 90\dot{z}_{-1} + 15\dot{z}_{-2}) \\ Z_{-3/2} &= \frac{1}{256}(12z_0 + 135z_{-1} + 108z_{-2} + z_{-3}) \\ &\quad + \frac{h}{256}(-3\dot{z}_n - 54\dot{z}_{n-1} + 27\dot{z}_{n-2}) \end{aligned} \tag{2-30}$$

The coding of the predictor–corrector integration method was checked using the sample problem given by Ralston and Wilf [15, p. 108]. Preliminary comparisons of

the performance of the Runge–Kutta and predictor–corrector methods are described in the following section.

2.3.4 Integrations of Some Simplified Particle Trajectories

Tests of the two integration methods were performed first on Eq. (2-23) using Davies equations [3] for particle terminal velocity, $W[t, z(t)]$, and Eqs. (2-1), (2-2), and (2-3) for the vertical distribution of density, viscosity, and mean free path. Typical results are shown in Table 2-3, which lists computed heights as a function of time for a 97-micron diameter sphere (density 5) falling from 29 km. No changes in step length were permitted during integration by the predictor–corrector method in this test. The first few values are identical for both methods, because the Runge–Kutta method was used for starting. It is clear from Table 2-3 that both methods yielded accurate results even for the largest time step. At $t = 2 \times 10^4$ sec, the greatest variation in height estimates was about 0.05 km or less than 0.2 percent of the total distance of fall. The fall time of 2.10×10^4 sec from 29 km to 0.3 km compares reasonably well with the total time of 2.19×10^4 sec obtained with Model A for the fall of a similar sphere from 30 km to the earth's surface.

For most particle sizes of interest the terminal velocity increases monotonically with altitude. The zonal wind speed $\dot{\lambda}$, on the other hand, may be characterized by several minima and maxima representing easterly and westerly wind layers. The following equation was used to represent $\dot{\lambda}$ for initial test purposes:

$$\dot{\lambda} = A \sin kz \tag{2-31}$$

with the maximum wind speed $A = 7.87 \times 10^{-6}$ rad sec^{-1} (50 m sec^{-1}) and $k = 2\pi/15$. The wind profile given by Eq. (2-31) is shown in Fig. 2-6 (for latitude 0°).

Using Davies' [3] equations for terminal velocity and Eq. (2-31) for zonal wind speed, the height z and longitude λ were computed for a 97-micron diameter sphere (density 5) as functions of time by the Runge–Kutta and predictor–corrector methods. The results for time step $h = 10^3$ sec are listed in Table 2-4. The criteria used for changing time-step length in the predictor–corrector method were as follows:

$$\sum_i \ell^i \left| p_r^i - c_r^i \right| \le m_1 \qquad (i = 1, 2, 3) \tag{2-32}$$

TABLE 2-3

PARTICLE ALTITUDE [z, (km)] AS A FUNCTION OF TIME (t) AS COMPUTED BY NUMERICAL INTEGRATION USING THE RUNGE–KUTTA (R–K) AND PREDICTOR–CORRECTOR (P–C) FOURTH-ORDER METHODS WITH VARIOUS TIME STEPS (h). (97-micron diameter sphere, density 5)

t	h = 100		h = 500		h = 1000		h = 5000	
($\times 10^{-3}$ sec)	R–K	P–C	R–K	P–C	R–K	P–C	R–K	P–C
0	29.000	29.000	29.000	29.000	29.000	29.000	29.000	29.000
1	27.211	27.211	27.211	27.211	27.211	27.211	–	–
2	25.452	25.452	25.452	25.452	25.452	25.452	–	–
3	23.729	23.729	23.729	23.729	23.729	23.729	–	–
4	22.046	22.046	22.046	22.046	22.046	22.046	–	–
5	20.403	20.404	20.403	20.407	20.408	20.404	20.392	20.392
6	18.797	18.797	18.796	18.800	18.801	18.793	–	–
7	17.239	17.240	17.239	17.242	17.244	17.238	–	–
8	15.730	15.731	15.730	15.733	15.734	15.728	–	–
9	14.267	14.267	14.266	14.269	14.271	14.262	–	–
10	12.843	12.844	12.842	12.845	12.847	12.841	12.833	12.833
11	11.447	11.448	11.445	11.454	11.456	11.448	–	–
12	10.100	10.101	10.099	10.106	10.108	10.093	–	–
13	8.8182	8.8194	8.8170	8.8239	8.8264	8.8185	–	–
14	7.6001	7.6013	7.5990	7.6055	7.6079	7.5982	–	–
15	6.4410	6.4420	6.4398	6.4461	6.4482	6.4408	6.4401	6.4401
16	5.3275	5.3286	5.3264	5.3324	5.3345	5.3264	–	–
17	4.2552	4.2562	4.2541	4.2599	4.2619	4.2543	–	–
18	3.2201	3.2211	3.2191	3.2246	3.2266	3.2191	–	–
19	2.2190	2.2199	2.2180	2.2234	2.2253	2.2181	–	–
20	1.2491	1.2500	1.2481	1.2533	1.2552	1.2482	1.2483	1.2860
21	0.3079	0.3088	0.3070	0.3120	0.3138	0.3070	–	–

$$\sum_i \ell^i \left| p_r^i - c_r^i \right| \geq m_2 \qquad (i = 1, 2, 3) \qquad (2\text{-}33)$$

$$\sum_i \ell^i \left| p_r^i - c_r^i \right| > m_3 \qquad (i = 1, 2, 3) \qquad (2\text{-}34)$$

where $\left| p_r^i - c_r^i \right|$ represents the absolute value of the difference between the predictor and the corrector at the r^{th} time step along coordinate i and where ℓ and m are constants assigned the following numerical values:

$$\ell^1 (z) = 1.0 \qquad m_1 = 6 \times 10^{-4}$$

$$\ell^2 (\lambda) = 0.08 \qquad m_2 = 6 \times 10^{-3}$$

$$\ell^3 (\theta) = 0 \qquad m_3 = 3 \times 10^{-2}$$

The constants ℓ^i above are weighting factors that permit proper apportionment of the individual step errors among the three coordinates. The constants m_1, m_2, and m_3 represent the criteria for doubling the time step, halving the time step, and stopping computations, respectively.

Time step length changes occurred at $t = 4 \times 10^3$ sec (doubled) and again at $t = 10^4$ sec (halved) with the predictor–corrector method in Table 2-4. As expected, the oscillatory nature of the zonal wind profile resulted in much larger differences between simultaneous values of λ computed by the two methods than those found for z (see Table 2-3). The zonal positions of the particle given by the Runge–Kutta integrations are shown in Fig. 2-6 (right side).

Because the integrations listed in Table 2-4 are based on Davies' equations for terminal velocity, the correct solutions for z and λ are not known exactly. Thus, the following simplified equation was used for terminal velocity:

$$\dot{z} = W_T - \Omega/t \qquad (2\text{-}35)$$

where Ω is a constant. Equations (2-31) and (2-35) can be integrated to give the following explicit expressions for z and λ:

$$z = \Omega \ln t + C_1 \qquad (2\text{-}36)$$

$$\lambda = \frac{At}{[1 + (k\Omega)^2]} \cos k C_1 \left\{ \sin (k\Omega \ln t) - (k\Omega) \cos (k\Omega \ln t) \right\} + \frac{Ak\Omega t}{[1 + (k\Omega)^2]} \sin k C_1 \left\{ \sin (k\Omega \ln t) + \frac{1}{(k\Omega)} \cos (k\Omega \ln t) \right\} + C_2 \qquad (2\text{-}37)$$

TABLE 2-4

ALTITUDES (z) AND LONGITUDES (λ) AS FUNCTIONS OF TIME (t) BY THE RUNGE-KUTTA (R-K) AND PREDICTOR-CORRECTOR (P-C) METHODS USING A TIME STEP OF 10^3 sec FOR A 97-micron DIAMETER SPHERE FALLING THROUGH A HEIGHT-DEPENDENT ZONAL WIND FIELD

t ($\times 10^{-3}$ sec)	z (km)	$\lambda-\lambda_0$ ($\times 10^3$ RAD.)	
		R-K	P-C
0	30.0	0	0
1	28.2	- 2.8232	- 2.8232
2	26.4	- 9.7404	- 9.7404
3	24.7	-17.076	-17.076
4	23.0	-21.078	-21.069
5	21.3	-19.816	–
6	19.6	-13.980	-13.960
7	18.0	- 6.2884	–
8	16.5	- 0.042474	- 0.010416
9	15.0	+ 2.3142	–
10	13.6	+ 0.010490	+ 0.039055
11	12.2	- 6.0259	–
12	10.8	-13.723	-14.383
13	9.5	-20.678	-21.338
14	8.3	-24.924	-25.587
15	7.1	-25.443	-26.108
16	5.9	-22.262	-22.933
17	4.8	-16.218	-16.895
18	3.8	- 8.6432	- 9.3228
19	2.7	- 1.0289	- 1.7067
20	1.8	+ 5.2739	+ 4.6013
21	0.8	+ 9.2608	+ 8.5955

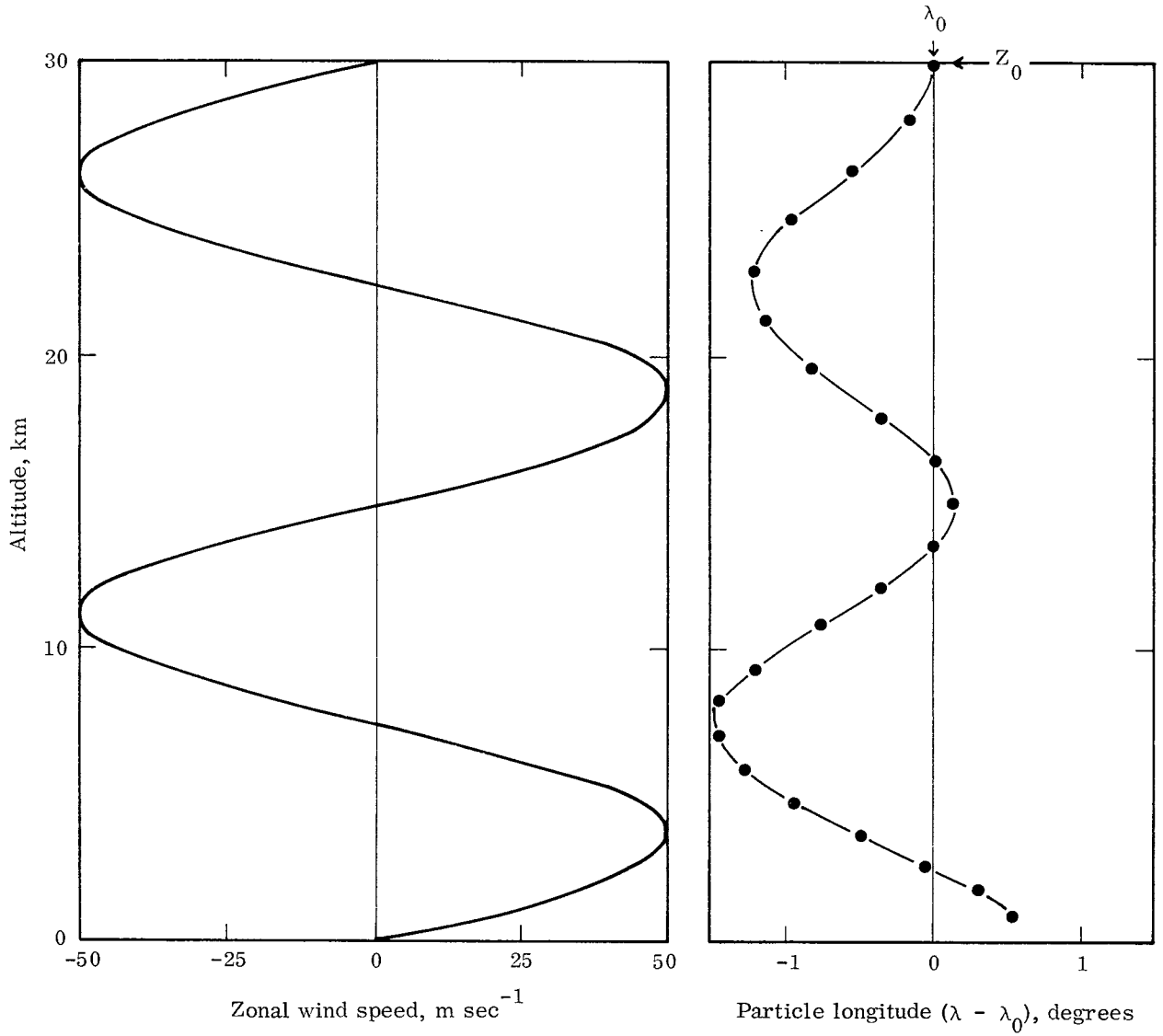

Fig. 2-6. Idealized zonal wind profile (left) and particle trajectory (right) computed by Runge—Kutta numerical integration (time step = 10^3 sec).

where

$$C_1 = z_0 - \Omega \ell n\, t_0 \tag{2-38}$$

and

$$C_2 = \frac{-A}{[1 + (k\Omega)^2]} \{\sin k z_0 - (k\Omega) \cos k z_0\} \tag{2-39}$$

The various constants in Eqs. (2-36) and (2-37) can be interpreted as follows. A particle is released at time t_0 from altitude z_0 with an initial terminal velocity Ω. It falls at decreasing speed through alternating layers of easterly and westerly winds. The maximum zonal wind speed in each layer is given by A and the total number of wind layers between the earth's surface and z_0 is kz_0/π. For the choice $z_0 = 30$ km, $t_0 = 1.0$ hr, and $\Omega = -30$ km hr^{-1}, the terminal velocity varies with altitude according to

$$z = W_T = -30 \exp\left(\frac{z - z_0}{30}\right) \tag{2-40}$$

Equation (2-40) is illustrated in Fig. 2-7. The remaining constants were assigned the values $A = 4.68 \times 10^{-2}$ rad hr^{-1} and $k = 2\pi/15$. The error criteria [Eqs. (2-32), (2-33), and (2-34)] were chosen to be:

$$\ell^1(z) = 1.0 \qquad m_1 = 0.003$$

$$\ell^2(\lambda) = 6.4 \times 10^2 \qquad m_2 = 0.03$$

$$\ell^3(\theta) = 0 \qquad m_3 = 0.15$$

The zonal components of the particle trajectory computed by the Runge–Kutta and predictor–corrector methods using four different initial time steps are given in Table 2-5. The correct longitudes (rounded to 5 significant figures) from Eq. (2-37) are listed in the last column of the table. Due to changes in step length during the integration, predictor–corrector estimates were not available for all selected times. The number of time steps in the bottom row of the table refers to all computations between $t = 1.000$ and $t = 2.624$ hr.

For the largest time step ($h = 0.232$ hr), predictor–corrector computations were terminated at $t = 2.1$ hr due to excessive errors. In terms of both accuracy and speed, the performance of the Runge–Kutta method was superior to the predictor–

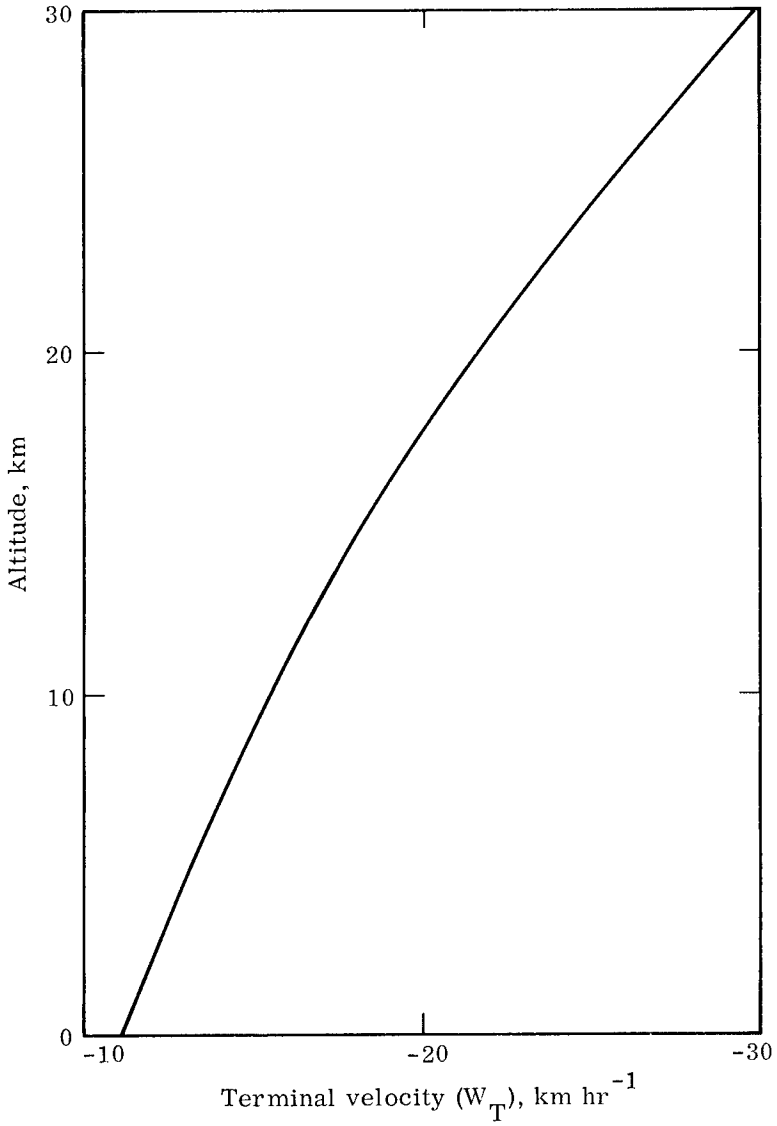

Fig. 2-7. Simulated particle terminal velocity as a function of altitude for trajectory integration tests.

TABLE 2-5

PARTICLE LONGITUDES [λ ($\times 10^3$ rad)] AS A FUNCTION OF TIME (t) FOR A PARTICLE FALLING THROUGH A VARIABLE ZONAL WIND FIELD. (NUMERICAL INTEGRATIONS BY A RUNGE–KUTTA (R–K) AND A PREDICTOR–CORRECTOR (P–C) METHOD WITH TIME STEP (h)

t (hr)	λ ($\times 10^3$ rad) by numerical integration								λ($\times 10^3$ rad) by exact integration
	h = 0.029		h = 0.058		h = 0.116		h = 0.232		
	R–K	P–C	R–K	P–C	R–K	P–C	R–K	P–C	
1.000	0	0	0	0	0	0	0	0	0
1.116	- 3.2369	- 3.2369	- 3.2372	- 3.2372	- 3.2428	- 3.2428	—	—	- 3.2367
1.232	- 7.8383	—	- 7.8388	- 7.8351	- 7.8467	- 7.8467	- 7.9874	- 7.9874	- 7.8382
1.348	- 7.5591	- 7.5545	- 7.5595	—	- 7.5660	- 7.5660	—	—	- 7.5592
1.464	- 2.8511	- 2.8463	- 2.8514	—	- 2.8559	- 2.6985	- 2.9353	- 2.9353	- 2.8512
1.580	+ 1.5666	—	+ 1.5664	+ 1.5698	+ 1.5625	+ 1.7214	—	—	+ 1.5666
1.696	+ 2.0100	—	+ 2.0097	—	+ 2.0055	+ 2.1649	+ 1.9283	+ 1.9283	+ 2.0100
1.812	- 1.6825	—	- 1.6828	- 1.6802	- 1.6879	- 1.5277	—	—	- 1.6824
1.928	- 6.9746	—	- 6.9749	- 6.9720	- 6.9805	- 6.8195	- 7.0796	- 9.8322	- 6.9745
2.044	-10.799	—	-10.799	-10.795	-10.805	-10.643	—	—	-10.798
2.160	-11.282	—	-11.282	—	-11.288	—	-11.386	Error criterion exceeded	-11.282
2.276	- 8.3409	—	- 8.3412	- 8.3174	- 8.3465	- 8.1651	—		- 8.3408
2.392	- 3.3160	—	- 3.3163	- 3.2934	- 3.3214	- 3.1410	- 3.4109	—	- 3.3161
2.508	+ 1.8479	—	+ 1.8476	+ 1.8702	+ 1.8427	+ 2.0226	—	—	+ 1.8479
2.624	+ 5.4019	—	+ 5.4016	—	+ 5.3967	—	+ 5.3102	—	+ 5.4019
2.711	+ 6.3532	+ 6.3682	—	—	—	—	—	—	+ 6.3532
Number of time steps	56	32	28	28	14	27	7	—	—

corrector method for this problem. In computations performed by the latter method, large errors appeared first during changes in step length.

For a final series of trajectory integration tests, a third equation for north–south particle motions was added to those previously used for the east–west and vertical components of motion.

$$\dot{\theta} = B \sin Kt \sin M\theta \tag{2-41}$$

Integration of Eq. (2-41) gives

$$\theta = \frac{2}{M} \tan^{-1} \exp - M \left\{ \frac{B}{K} \cos Kt - C_3 \right\} \tag{2-42}$$

where

$$C_3 = \frac{1}{M} \left\{ \ell n \tan \frac{M\theta_0}{2} + \frac{B}{K} \cos K \right\} \tag{2-43}$$

The constant B is the maximum meridional wind speed. The number of complete waves in the north–south component of particle motion between the initial altitude z_0 and the earth's surface is $K z_0/\pi$.

A total of four tests were performed using the Runge–Kutta method with variations in θ_0, B, and the step length h. Input parameters for the tests are listed in Table 2-6. The values of k and K in Table 2-6 specify six wind layers in the vertical and twenty waves in the meridional component of motion of the particle between 90 km and the earth's surface. The initial co-latitude, θ_0, and maximum meridional wind speed, B, in Tests 1 and 2 were chosen to yield large round-off errors in order to test the behavior of the integration methods under such conditions. The results of Tests 1 and 2 are given in Table 2-7.

It is evident from Table 2-7 that the numerical integrations were less accurate for the oscillatory functions for $\dot{\theta}$ and $\dot{\lambda}$ than for the monotonic function for terminal velocity W_T. The errors in λ appeared to be due primarily to truncation, because their magnitudes increased as the time step length was increased. The opposite occurred for θ errors, however, as they were due primarily to round-off. The Runge–Kutta estimates of θ were well-behaved, with no indication for instability even with a relatively large time step length. The time step length h = 0.24 hr corresponded to approximately 0.24 x(20/12) = 0.4 times the wave-length of the oscillations in the north–south component of motion of the particle.

TABLE 2-6
INPUT PARAMETERS FOR THREE-DIMENSIONAL
TRAJECTORY COMPUTATIONS

Parameter	Test number			
	1	2	3	4
Ω(km hr^{-1})	-36	-36	-36	-36
t_0 (hr)	1.0	1.0	1.0	1.0
z_0 (km)	90	90	90	90
λ_0 (rad)	0	0	0	0
θ_0 (rad)	0.1	0.1	$\pi/2$	$\pi/2$
A (rad hr^{-1})	7.87×10^{-2}	7.87×10^{-2}	7.87×10^{-2}	7.87×10^{-2}
B (rad hr^{-1})	3.94×10^{-5}	3.94×10^{-5}	1×10^{-2}	1×10^{-2}
M	1.0	1.0	1.0	1.0
k	0.21	0.21	0.21	0.21
K	11	11	11	11
h (hr)	0.12	0.12	0.12	0.12

In Tests 3 and 4, the parameters θ_0 and B were increased to reduce round-off errors. The results of exact and numerical integrations of θ (Runge–Kutta method) for this problem are listed in Table 2-8. Here the θ errors increased with an increase in step length, but even with a step length of 0.24 hr, the largest errors were not more than 3 percent of the maximum deviation of the particle from the source latitude.

Tests 1 to 4 will be repeated with the predictor–corrector method of integration in December. Following this, tests will be performed using the simulated zonal wind fields discussed in Section 3.0 of this report.

TABLE 2-7

PARTICLE POSITIONS (z, λ, θ) AS A FUNCTION OF TIME (t) BY EXACT INTEGRATION AND BY RUNGE–KUTTA (R–K) NUMERICAL INTEGRATION USING TWO TIME STEPS (h)

t (hr)	z (km)			$\lambda-\lambda_0$ (× 10^2 rad)			$\theta-\theta_0$ (× 10^7 rad)		
	exact	h = 0.12	h = 0.24	exact	h = 0.12	h = 0.24	exact	h = 0.12	h = 0.24
1.00	90.000	90.000	90.000	0	0	0	0	0	0
1.48	75.886	75.886	75.886	- 2.5549	- 2.5552	- 2.5586	+ 2.80	+ 3.20	+ 3.00
1.96	65.774	65.774	65.774	- 0.0652	- 0.0654	- 0.0675	+ 4.20	+ 4.70	+ 4.40
2.44	57.888	57.888	57.888	+ 1.0941	+ 1.0939	+ 1.0916	+ 3.00	+ 3.50	+ 3.10
2.92	51.423	51.423	51.423	- 2.0829	- 2.0831	- 2.0856	+ 0.10	+ 0.60	+ 0.20
3.40	45.944	45.944	45.944	- 4.5362	- 4.5364	- 4.5389	- 2.34	- 1.59	- 2.19
3.88	41.190	41.190	41.190	- 3.4264	- 3.4265	- 3.4290	- 2.54	- 1.64	- 2.33
4.36	36.991	36.991	36.991	+ 0.0400	+ 0.0398	+ 0.0374	- 0.26	+ 0.50	0.00
4.84	33.231	33.231	33.231	+ 3.2572	+ 3.2571	+ 3.2546	+ 2.60	+ 3.50	+ 3.10
5.32	29.827	29.827	29.827	+ 4.4014	+ 4.4012	+ 4.3988	+ 4.20	+ 4.90	+ 4.70
5.80	26.717	26.717	26.717	+ 3.0710	+ 3.0708	+ 3.0684	+ 3.20	+ 3.90	+ 3.70
6.28	23.855	23.855	23.855	- 0.0428	- 0.0430	- 0.0454	+ 0.30	+ 1.20	+ 0.80
6.76	21.203	21.203	21.203	- 3.7720	- 3.7722	- 3.7747	- 2.24	- 1.30	- 1.79
7.24	18.734	18.734	18.734	- 6.9891	- 6.9893	- 6.9918	- 2.54	- 1.85	- 2.05
7.72	16.423	16.423	16.423	- 8.9039	- 8.9041	- 8.9066	- 0.46	+ 0.40	+ 0.10
8.20	14.251	14.251	14.251	- 9.1594	- 9.1596	- 9.1620	+ 2.40	+ 3.50	+ 3.30
8.68	12.203	12.203	12.203	- 7.7921	- 7.7923	- 7.7948	+ 4.20	+ 5.20	+ 5.00
9.16	10.266	10.266	10.266	- 5.1258	- 5.1260	- 5.1284	+ 3.30	+ 4.30	+ 4.20
9.64	8.427	8.427	8.427	- 1.6463	- 1.6465	- 1.6489	+ 0.50	+ 1.70	+ 1.40
10.12	6.678	6.678	6.678	+ 2.1100	+ 2.1098	+ 2.1074	- 2.04	- 0.97	- 1.19
10.60	5.009	5.009	5.009	+ 5.6428	+ 5.6426	+ 5.6401	- 2.64	- 1.42	- 1.75
11.08	3.415	3.415	3.415	+ 8.5430	+ 8.5428	+ 8.5404	- 0.64	+ 0.70	+ 0.20
11.56	1.888	1.888	1.888	+10.523	+10.522	10.520	+ 2.30	+ 3.80	+ 3.30
12.04	0.424	0.424	0.424	+11.421	+11.421	11.418	+ 4.10	+ 5.70	+ 5.30
Number of time steps	–	92	46	–	92	46	–	92	46

TABLE 2-8

PARTICLE COLATITUDE (θ) AS A FUNCTION OF TIME (t) BY EXACT INTEGRATION AND BY RUNGE–KUTTA (R–K) NUMERICAL INTEGRATION USING TWO TIME STEPS (h)

t (hr)	z (km)	$\theta - \theta_0$ ($\times 10^4$ rad)		
		exact	h = 0.12	h = 0.24
1.00	90.0	0	0	0
1.48	75.9	+ 7.495	+ 7.507	+ 7.655
1.96	65.8	+11.028	+11.045	+11.268
2.44	57.9	+ 7.984	+ 7.998	+ 8.155
2.92	51.4	+ 0.614	+ 0.622	+ 0.618
3.40	45.9	- 5.630	- 5.629	- 5.771
3.88	41.2	- 6.132	- 6.131	- 6.284
4.36	37.0	- 0.520	- 0.512	- 0.540
4.84	33.2	+ 7.055	+ 7.073	+ 7.212
5.32	29.8	+10.993	+11.017	+11.239
5.80	26.7	+ 8.378	+ 8.402	+ 8.565
6.28	23.8	+ 1.148	+ 1.164	+ 1.167
6.76	21.2	- 5.353	- 5.344	- 5.484
7.24	18.7	- 6.316	- 6.305	- 6.469
7.72	16.4	- 1.029	- 1.010	- 1.058
8.20	14.2	+ 6.598	+ 6.625	+ 6.747
8.68	12.2	+10.925	+10.957	+11.175
9.16	10.3	+ 8.751	+ 8.781	+ 8.952
9.64	8.4	+ 1.685	+ 1.705	+ 1.722
10.12	6.7	- 5.048	- 5.034	- 5.167
10.60	5.0	- 6.469	- 6.453	- 6.621
11.08	3.4	- 1.527	- 1.503	- 1.563
11.56	1.9	+ 6.124	+ 6.160	+ 6.266
12.04	0.4	+10.825	+10.866	+11.076
Number of time steps		–	92	46

2.4 Mass-element Expansion and Subdivision

Computer program specifications were prepared for the subdivision of mass-elements forming both polydisperse and monodisperse particle clouds as outlined in the first quarterly progress report issued under this project [9]. Coding of this subroutine was delayed pending completion of tests of trajectory integration methods.

2.5 Surface Deposit Densities and Air Concentrations

Preliminary specifications and coding were completed for establishing a grid at the earth's surface and at some level above the earth's surface for the purpose of analyzing surface deposit densities and air concentrations, respectively. A polar stereographic projection is used for latitudes poleward of 20 degrees and a Mercator projection for tropical latitudes. Verification of these components of the model have also been delayed until the trajectory routines have been completed.

3.0 ATMOSPHERIC AIR FLOW SIMULATION MODELS

3.1 Zonal Flow Representation

Examination of the least-squares polynomial approximations of the pole-to-pole zonal wind profiles obtained by the methods described in [9] has shown the most desirable fit to be the ninth-degree approximation. The choice of this polynomial was determined by its over-all accuracy in the latitudinal regions of greatest importance (70° N to 30° S) for the purposes of the project. In general, lower-degree approximations were found to give better results in the polar regions at the expense of close agreement with the observed profiles in the lower latitudes.

Figures 3-1 and 3-2 show the observed 500- and 200-mb profiles for two seasons as given by Mintz [12] plotted together with the corresponding 9th- and 5th- degree approximations. It is seen that an undesirable fluctuation occurs in the northern polar region for the 9th-degree curves, but that the 9th-degree polynomial gives an acceptable approximation for the remaining latitudes while the 5th-degree polynomial does not.

Figures 3-3 and 3-4 show the approximating profiles for the 30- and 60-km levels. Observed profiles were not available for these upper levels, but data were obtained [10] for the northern hemisphere (winter and summer) at various latitudes and interpolated to equally spaced intervals. Because no southern hemisphere data of this type were found, data for the northern hemisphere winter were taken for the southern hemisphere winter, etc. to obtain complete pole-to-pole profiles.

For each of the specified height levels $z = z_i$, ($i=1, 2, \ldots, \ell$, where ℓ is the total number of levels at which data are read off), the ninth-degree approximation to the zonal wind has the form

$$V_9(Z_i, \theta) = \sum_{k=0}^{9} a_k(Z_i)\, p_k(\theta) \qquad (i=1, 2, \ldots, \ell) \qquad (3\text{-}1)$$

where θ denotes colatitude. For a fixed value of k, each set of coefficients $a_k(z_1)$, $a_k(z_2)$, ..., $a_k(z_\ell)$ can be fitted by the same least-squares process as was used in the horizontal approximations to obtain a smooth vertical fitting of the pole-to-pole profiles. This method of fitting eliminates the possibility of encountering undesirable effects upon particle trajectories brought about by discontinuities in the vertical shear.

In order to take advantage of the greater resolution of data at the lower altitudes,

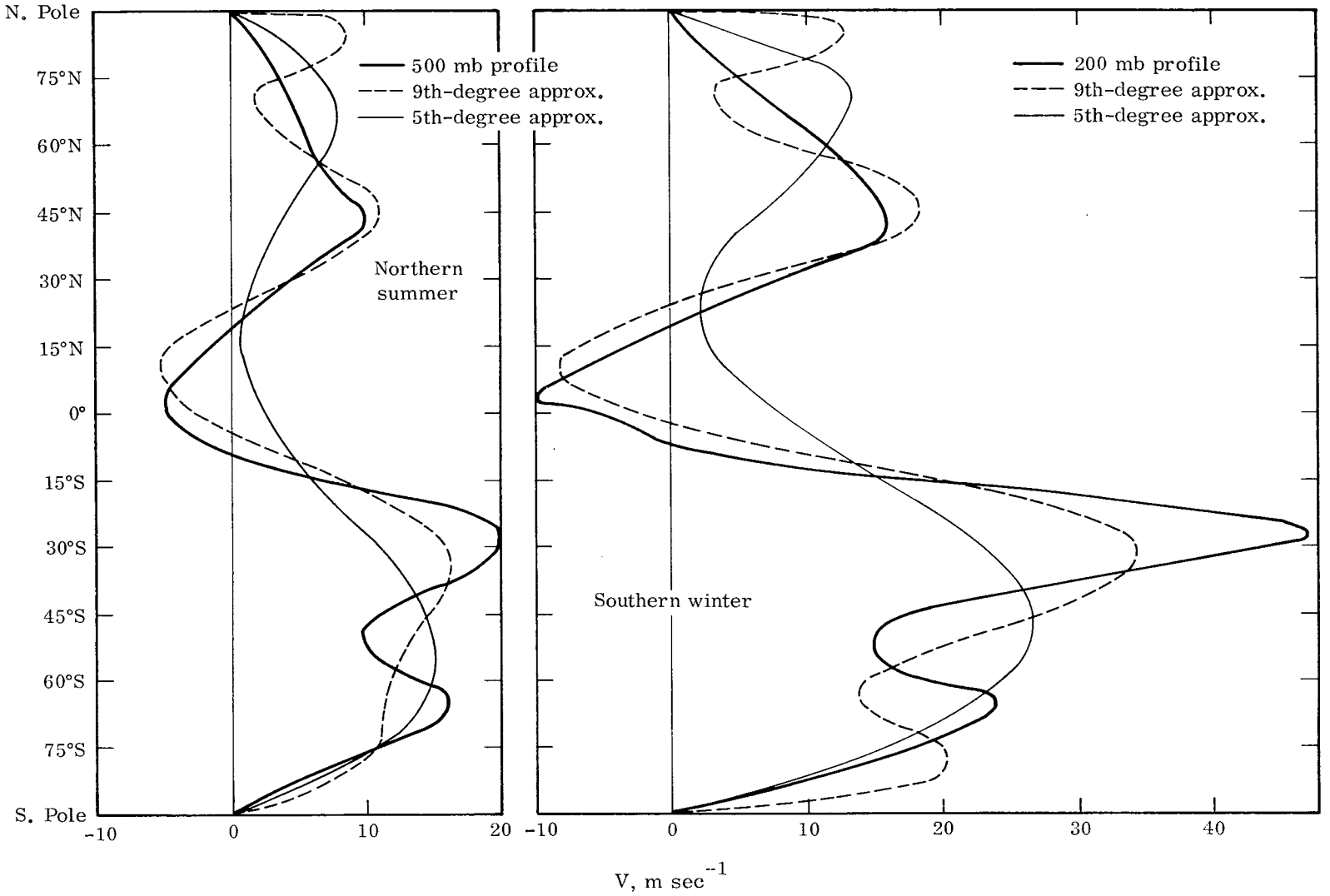

Fig. 3-1 a, b. The observed 500- and 200-mb pole-to-pole zonal wind profiles for the northern-hemisphere summer and southern-hemisphere winter, plotted together with the 5th- and 9th-degree approximations.

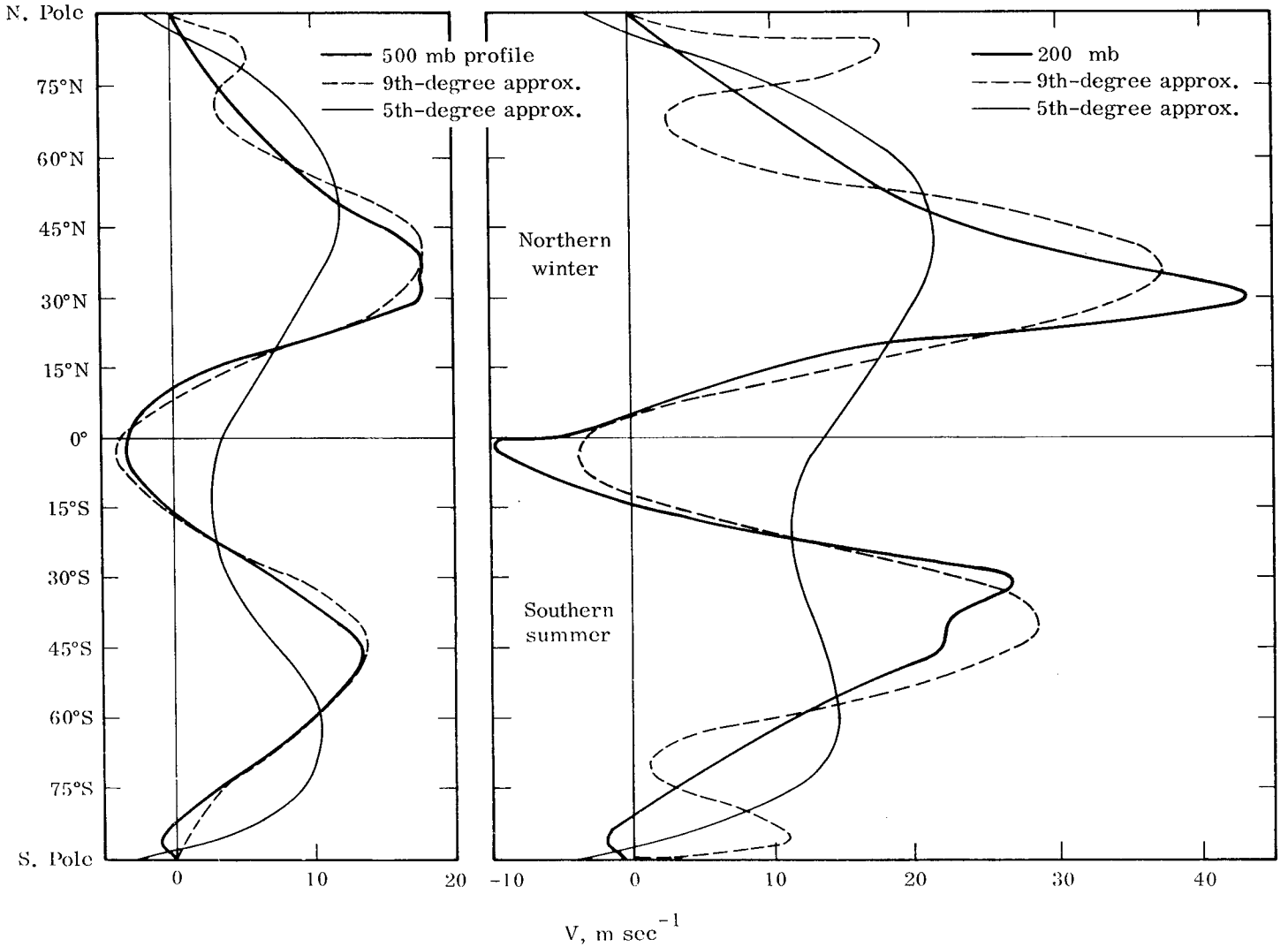

Fig. 3-2 a, b. The observed 500- and 200-mb pole-to-pole zonal wind profiles for the northern-hemisphere winter and southern-hemisphere summer plotted together with the 5th- and 9th-degree approximations.

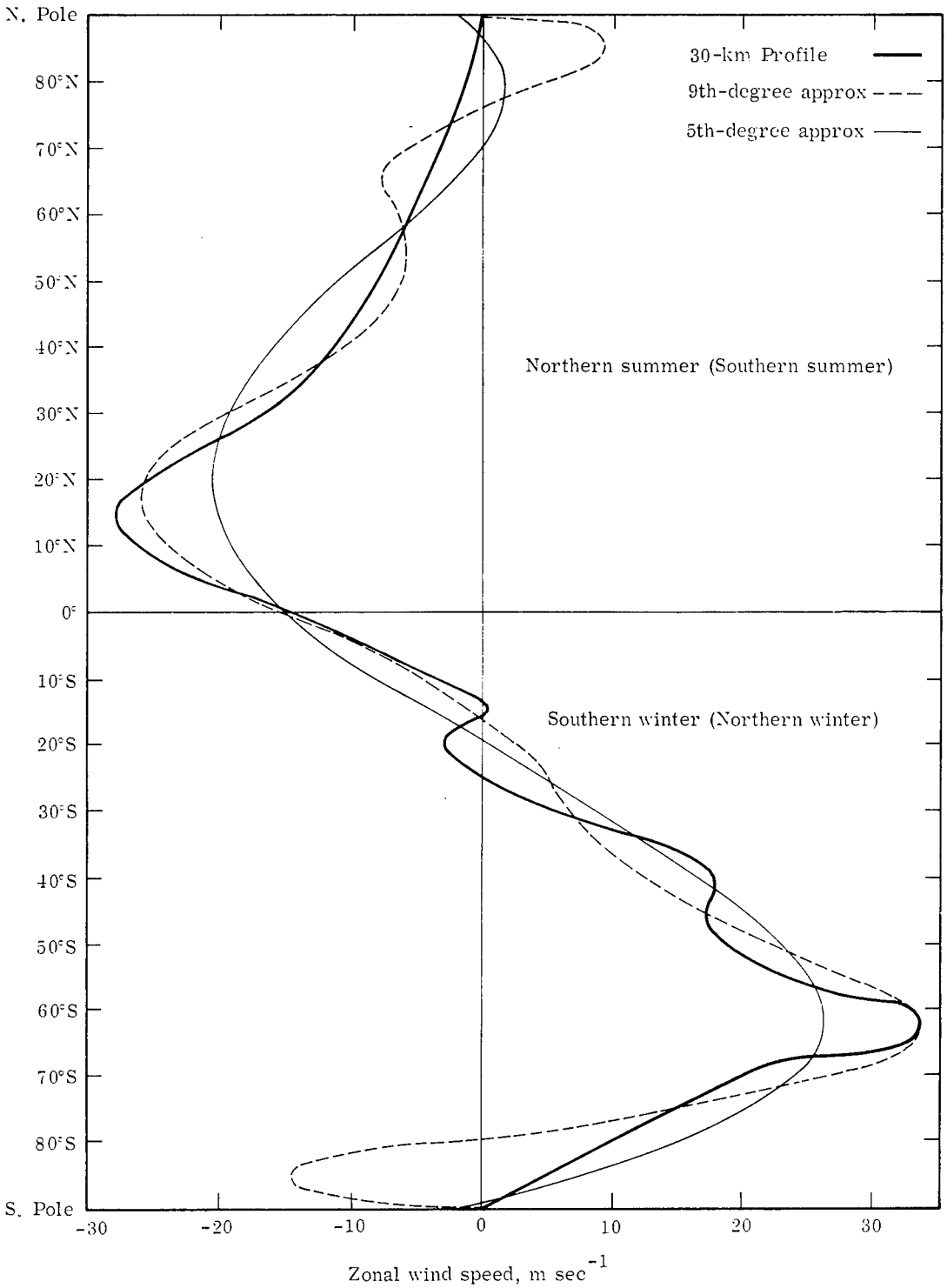

Fig. 3-3. The 30-km observed zonal wind values plotted together with the 5th- and 9th-degree approximations.

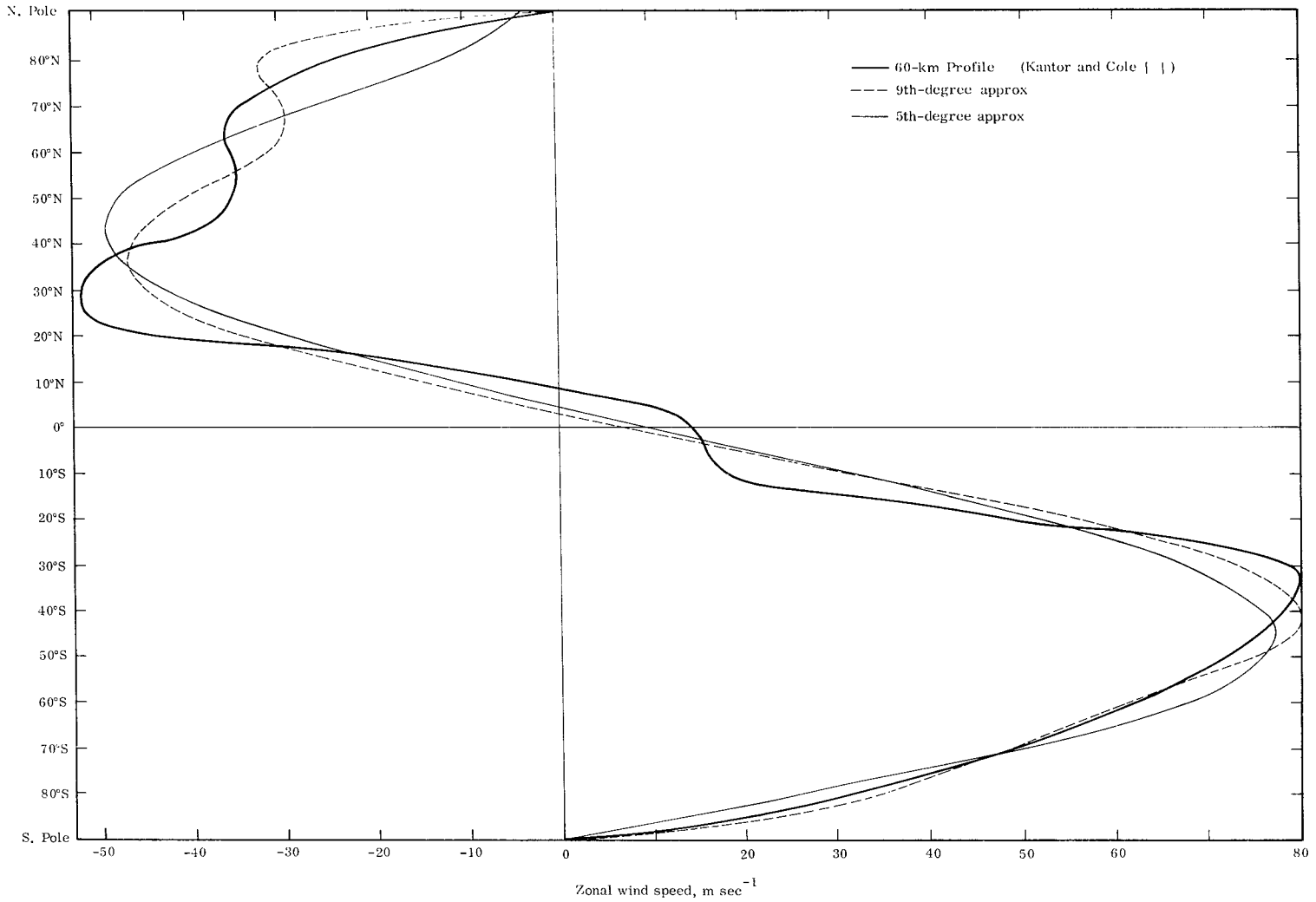

Fig. 3-4. The 60-km observed zonal wind values plotted together with the 5th- and 9th-degree approximations.

a change of height variable from z to z′ can be made to place the levels z_1', z_2', ..., z_1' at approximately equal spacing in the new variable z′. The transformation $z' = z^{1/2}$ accomplishes this purpose.

A computer program has been completed for calculating the zonal wind at any number of coordinate points (θ, z); thus vertical as well as pole-to-pole profiles can be readily calculated for comparison with observational data. Analysis of many such profiles will be necessary for determining the appropriate degree of approximation in the vertical least-squares fit.

3.2 Long Atmospheric Waves

In accordance with the formula

$$\Psi(\theta, \lambda) = \sum_m \sum_n A_n^m \cos\left[m(\lambda - \delta_n^m)\right] P_n^m(\cos\theta) \tag{3-2}$$

the stream function Ψ for the long-atmospheric waves has been computed at every ten degrees of latitude and longitude for the 1000- and 500-mb levels. The amplitudes A_n^m and phase angles δ_n^m which were used in the calculations are those given by Eliasen and Machenhauer [6] for a 90-day winter mean flow. As is customary, the long-wave numbers correspond to the values m = 1, 2, 3, 4, while in this case (n-m) takes on the values 1, 3, 5, 7. (Recall that m represents the number of waves around a circle of latitude, while n-m is the number of nodal points of $P_n^m(\theta)$ for $0 < \theta < \pi$.)

A computer subroutine for evaluating the associated Legendre functions $P_n^m(\cos\theta)$ was developed making use of the formula

$$P_n^m(\cos\theta) = \frac{(2n)!\sin^m\theta}{2^n n!(n-m)!}\left[\cos^{n-m}\theta - \frac{(n-m)(n-m-1)}{2(2n-1)}\cos^{n-m-2}\theta + \frac{(n-m)(n-m-1)(n-m-2)(n-m-3)}{(2)(4)(2n-1)(2n-3)}\cos^{n-m-4}\theta - + \ldots\right], \tag{3-3}$$

where the expression in the brackets ends with the a constant term if n-m is even and with the term containing cos θ if n-m is odd. This equation is that given by Byerly [2] and is basically the same as the one recommended for computational purposes by Fougere [7]. For verification of the results, values of the normalized associated Legendre function $\overline{P_n^m}$, which is related to P_n^m by the formula

$$\overline{P_n^m}(\cos\theta) = \left[\frac{(2n+1)}{2}\,\frac{(n-m)!}{(n+m)!}\right]^{1/2} P_n^m(\cos\theta) \qquad (3\text{-}4)$$

were computed for a number of n, m, and θ and compared to tabular values of this function given by Belousov [1]. In all cases the compared results were found to differ by less than 10^{-6}.

Figure 3-5 shows the stream lines at the high latitudes for the 1000-mb level obtained by analysis of the values of Ψ computed by Eq. (3-2) added to the values of the stream function corresponding to the 9th-degree approximation to the winter zonal flow at sea-level; the stream function $\overline{\Psi}$ for the zonal wind V_9 was computed by numerical integration of the relation

$$V_9 = \frac{1}{R}\,\frac{\partial\overline{\Psi}}{\partial\theta} \qquad (3\text{-}5)$$

where R is the earth's radius. Because the zonal winds are rather weak near the surface, the stream lines for the long-wave components are altered only slightly by the addition of $\overline{\Psi}$; for this reason, the map showing Ψ alone has been omitted.

At the 500-mb level, the effect of the zonal wind is substantial; Fig. 3-6 shows the stream lines for the long waves alone, while Fig. 3-7 shows the stream lines for the combined flow. In the latter case, the zonal wind dominates the flow to such an extent that nearly all the individual cells are smoothed into ridges and troughs, while only two closed lows are seen to retain their identities.

In Fig. 3-8, the stream lines for the combined flow at the 1000- and 500-mb levels are shown for the low-latitude belt from the equation to 30° N.

The vertical fitting of the long-wave components is to be done in a manner analogous to that of the zonal wind approximations, i.e., A_n^m and δ_n^m are to be taken as functions of the vertical coordinate z. Due to a lack of available data in regard to the long-wave components at the higher levels, the vertical fitting must be of a less precise nature than that described in the preceding section; nevertheless, some information concerning the behavior of the amplitudes and phase angles with height is available (Muench [13] and Eliasen [5]) for guidance in choosing an appropriate fit.

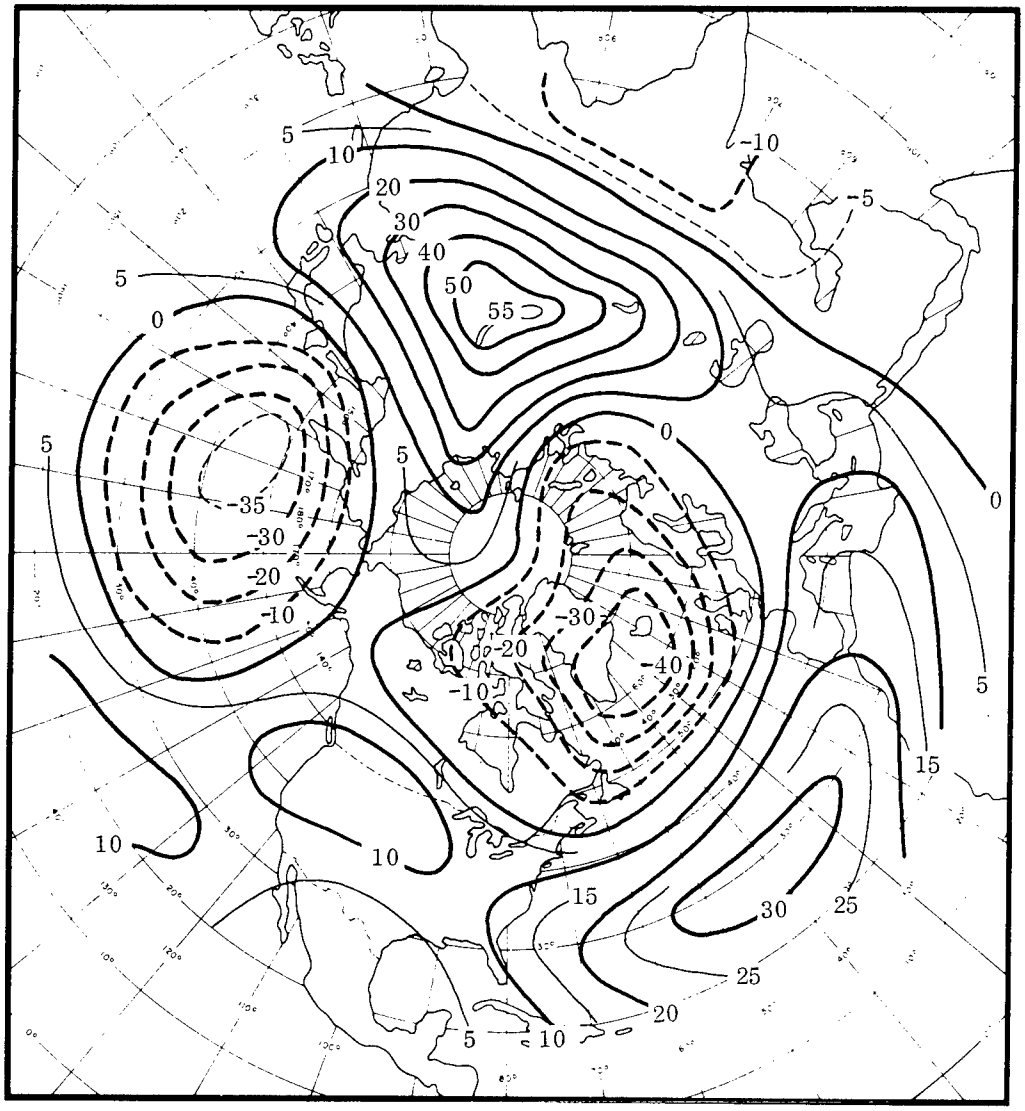

Fig. 3-5. The stream-lines of the northern-hemisphere zonal wind with long-wave wind components for the winter season at the 1000-mb level.

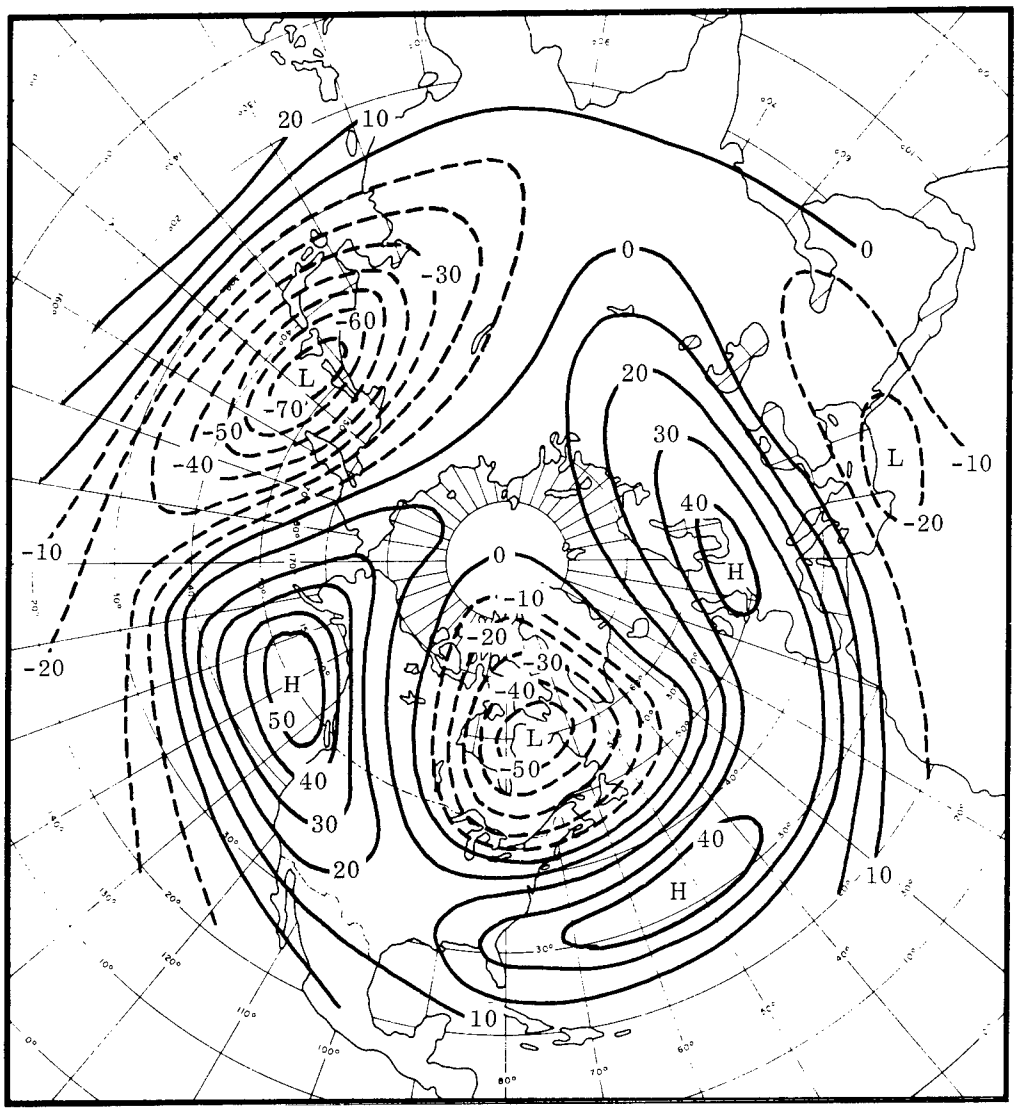

Fig. 3-6. The stream-lines of the northern-hemisphere long-wave wind components for the winter season at the 500-mb level.

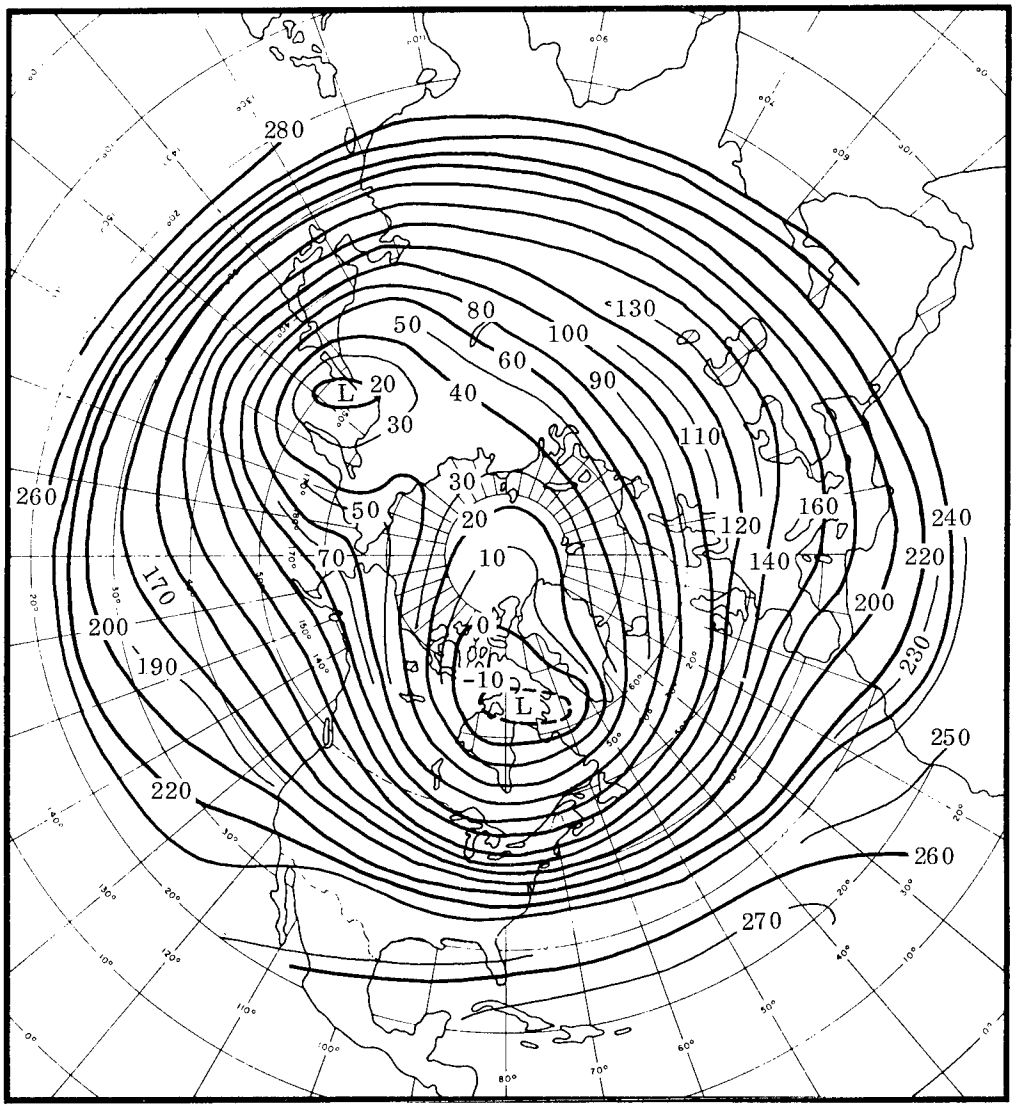

Fig. 3-7. The stream lines of the combined flow for the northern hemisphere at the 500-mb level.

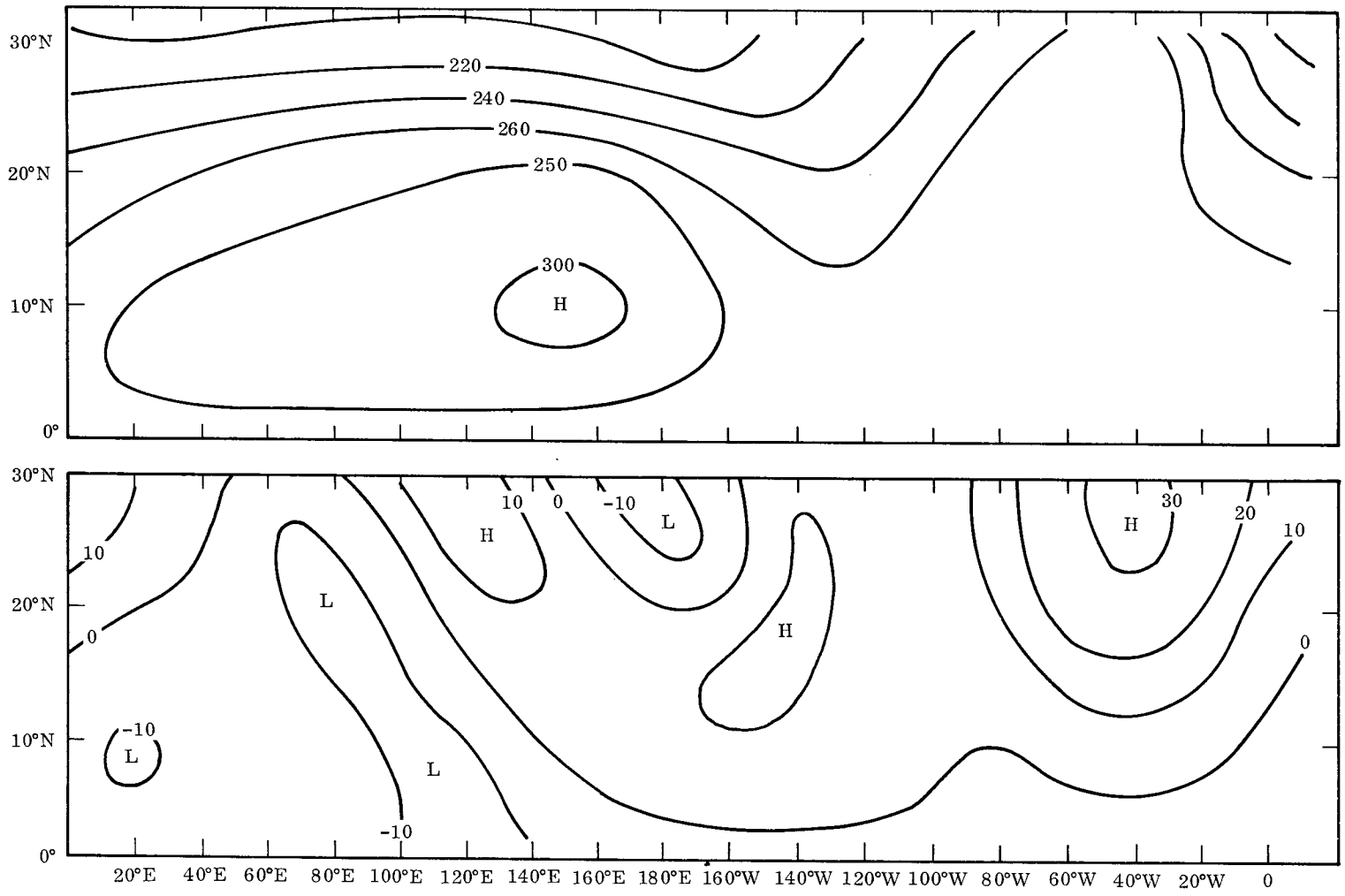

Fig. 3-8 a, b. The stream lines for the combined flow at the 1000- and 500-mb levels in the lower latitudes.

4.0 REFERENCES

1. Belousov, S. L., 1962: Tables of Normalized Associated Legendre Polynomials, Mathematical Tables Series, Vol. 18, Pergamon Press, MacMillan Co., New York.

2. Byerly, W. E., 1893: Fourier's Series and Spherical Harmonics. Ginn and Co., Boston.

3. Davies, C. N., 1945: "Definitive Equations for the Fluid Resistance of Spheres," Proc. Phys. Soc., Vol. 57, Part 4, pp. 259–270.

4. Duberg, J. E., W. J. O'Sullivan, Jr., R. A. Hord, S. L. Seaton, and J. A. Mullins, 1962: U.S. Standard Atmosphere, 1962, U.S. Government Printing Office, Washington, D.C.

5. Eliasen, E., 1958: "A Study of the Long Atmospheric Waves on the Basis of Zonal Harmonic Analysis," Tellus, Vol. 10, No. 2, pp. 206–215.

6. —, and B. Machenhauer, 1965: "A Study of the Fluctuations of the Atmospheric Planetary Flow Patterns Represented by Spherical Harmonics," Tellus, Vol. 17, No. 2, pp. 220–238.

7. Fougere, P. F., 1963: "Spherical Harmonic Analysis," J. Geophys. Res., Vol. 68, No. 4, pp. 1131–1139.

8. Gill, S., 1951: "A Process for the Step-by-Step Integration of Differential Equations in an Automatic Digital Computing Machine," Proc. Cambridge Phil. Soc., Vol. 47, pp. 96–108.

9. Hage, K. D., and P. S. Brown, 1965: Particle Fallout and Dispersion in the Atmosphere, Quart. Rpt. No. 1, Sandia Corporation, Contract 48-2417, The Travelers Research Center, Inc., 18 pp.

10. Hamming, R. W., 1959: "Stable Predictor Corrector Methods for Ordinary Differential Equations," J. Assoc. Comp. Mach., Vol. 6, pp. 37–47.

11. Kantor, A. J., and A. E. Cole, 1964: "Zonal and Meridional Winds to 120 Kilometers," J. Geophys. Res., Vol. 69, No. 24, pp. 5131–5140.

12. Mintz, Y., 1954: "The Observed Zonal Circulation of the Atmosphere," Bull. Am. Meteorol. Soc., Vol. 35, No. 5, pp. 208–214.

13. Muench, H. S., 1965: Stratospheric Energy Processes and Associated Atmospheric Long-wave Structure in Winter, Environmental Research Paper No. 95, U.S. Air Force Cambridge Research Center.

14. Öpik, E. J., 1958: Physics of Meteor Flight in the Atmosphere, Interscience Publishers, Inc., New York, 174 pp.

15. Ralston, A., and H. S. Wilf (Ed.), 1964: Mathematical Methods for Digital Computers, John Wiley and Sons, New York, 293 pp.

DISTRIBUTION:

U. S. Atomic Energy Commission
Albuquerque Operations Office
P. O. Box 5400
Albuquerque, New Mexico 87115
Attn: V. C. Vespe, Director
Operational Safety Division

USAEC, DSNS
Washington, D. C. 20545
Attn: G. P. Dix, Chief, Safety Branch SEPO (1)
W. A. Yingling, SNPO (1)
R. T. Carpenter, Chief, Isotopic Power System Branch, SEPO (1)
C. E. Johnson, Chief, Reactor Power Systems Branch, SEPO (1)

USAEC
Division of Reactor Development and Technology
Washington, D.C. 20545
Attn: J. A. Lieberman

USAEC
Office of the Assistant General
Council for Patents
Washington, D.C. 20545
Attn: Roland A. Anderson

USAEC
Division of Isotope Development
Washington, D.C. 20545
Attn: A. Berman (1)
J. A. Powers, For: W. K. Kern (1)

USAEC
Division of Military Application
Washington, D.C. 20545
Attn: Brig. General D. L. Crowson, USAF

USAEC
Division of Biology and Medicine
Washington, D.C. 20545
Attn: H. D. Bruner, Asst. Director
Medical and Health Research (1)
Dr. Roger McClellan (1)
J. Z. Holland, Chief, Fallout Studies Br. (1)

USAEC
Reactor Division of Safety Standards
Washington, D.C. 20545
Attn: J. J. Dinunno, Asst. Director

USAEC
Director of Regulation
Washington, D.C. 20545
Attn: H. L. Price

USAEC
DSNS, Space Nuclear Prop. Office
Washington, D.C. 20545
Attn: R. S. Decker, Jr., Chief, Safety Branch

USAEC
Division of Technical Information
Headquarters Library, G-017
Washington, D.C. 20545 (3)

Space Nuclear Propulsion Office
Lewis Research Center
21000 Brookpark Road
Cleveland, Ohio 44135
Attn: L. Nichols

USAEC New York Operations Office
376 Hudson Street
New York, New York 10014
Attn: A. L. Rizzo, Health and Safety Lab. (1)
J. Harley, Health and Safety Lab. (1)
G. Silverman (1)
W. Sullivan (1)

USAEC Albuquerque Operations Office
P. O. Box 5400
Albuquerque, New Mexico 87115
Attn: S. A. Upson, Director, Research and Classification Division (1)

USAEC Canoga Park Area Office
P. O. Box 591
Canoga Park, California
Attn: J. V. Levy, Area Manager (1)
C. A. Malmstrom (1)

USAEC
San Francisco Operations Office
2111 Bancroft Way
Berkeley, California 94704
Attn: Technical Services Division

USAEC
Chicago Operations Office
9800 South Cass Avenue
Argonne, Illinois 60439
Attn: Chief, Office Services Branch

U. S. Atomic Energy Commission
Oak Ridge Operations Office
Mail and Document Accountability Section
P. O. Box E
Oak Ridge, Tennessee 37831
Attn: Director, Research and Development Div.

Headquarters
Air Force Systems Command (SCIZN)
Washington, D.C. 20331
Attn: Nuclear Safety Branch

Director Nuclear Safety (AFINS)
Chief, Reactor and Advanced Systems Division
Kirtland Air Force Base, New Mexico
Attn: Col. D. C. Jameson (AFINS-R)

DISTRIBUTION (cont):
Deputy, the Inspector General, USAF
Director Nuclear Safety
Kirtland Air Force Base, New Mexico
Attn: Col. George Ogburn (AFINSR)

Director
Air Force Weapons Laboratory
Kirtland Air Force Base
Albuquerque, New Mexico
Attn: WLIL
For: Lt. Col. M. N. Nold (WLRB) (1)
Lt. Col. H. L. Harris (WLAS) (1)

Space Systems Division
Air Force Unit Post Office
Los Angeles, California 90045
Attn: Technical Library

Air University Library
Maxwell Air Force Base, Alabama
Attn: Elizabeth C. Perkins, AUL3T-7143

Armed Forces Radiobiology Research Ins.
Defense Atomic Support Agency
Washington, D.C. 20014
Attn: Library

Atomics International
P.O. Box 309
Canoga Park, California 91304
Attn: R. L. Detterman (2)

Atomics International
Div. North American Aviation, Inc.
1629 K Street NW
Washington, D.C.
Attn: Miles Huntsinger, Washington Representative

Battelle Memorial Institute
505 King Avenue
Columbus, Ohio 43201

Battelle Memorial Institute
Pacific Northwest Laboratory
P.O. Box 999
Richland, Washington 99352
Attn: Dr. Roy Thompson

Brookhaven National Laboratory
Technical Information Division
Upton, Long Island, New York 11973
Attn: Research Library

The Boeing Company
P.O. Box 3707
Seattle, Washington 98124
Attn: Maynard D. Pearson, Aero-Space Division

Chief, Defense Atomic Support Agency
P.O. Box 2610
Washington, D.C. 20301
Attn: Document Library Branch

Douglas Aircraft Company, Inc.
Missile and Space Systems Division
3000 Ocean Park Boulevard
Santa Monica, California
Attn: Sid Gromich, Advanced Space Technology

Edgerton, Germeshausen and Grier, Inc.
P.O. Box 98
Goleta, California

E. I. du Pont de Nemours and Company
Savannah River Laboratory
Aiken, South Carolina 29802
Attn: W. B. Scott, Document Division

General Atomic Division
General Dynamics Corporation
P.O. Box 608
San Diego, California 92112
Attn: Library

General Electric Company
570 Lexington Avenue
New York, New York 10022
Attn: Richard W. Porter, Consultant
Aerospace Science and Technology

General Electric Company
Valley Force Space Technology Center
Philadelphia, Pennsylvania
Attn: Carl Gamertsfelder, Advanced Requirements
Planning Department

General Electric Company
Valley Forge Space Technology Center
Philadelphia, Pennsylvania
Attn: S. M. Scala

Hittman Associates
P.O. Box 2685
4715 East Wabash Avenue
Baltimore, Maryland

Lockheed Missiles and Space Company
P.O. Box 504
Sunnyvale, California
Attn: H. H. Greenfield, Manager
Nuclear Power Development (1)
Dr. R. C. Lee (1)
Harold F. Plank (1)

Los Alamos Scientific Laboratory
P.O. Box 1663
Los Alamos, New Mexico 87544
Attn: Report Librarian (2)
Dr. L. D. P. King (1)
Dr. Wright Langham (1)

Lovelace Foundation for Medical Education
and Research
5200 Gibson Blvd., SE
Albuquerque, New Mexico
Attn: Dr. Clayton S. White, Director of Research

DISTRIBUTION (cont):

Martin Company Nuclear Division
Middle River, Maryland 21203
Attn: D. G. Harvey (1)
W. Vogele (1)

Minnesota Mining and Manufacturing Company
P.O. Box 6505
St. Paul, Minnesota
Attn: H. C. Zeman, Security Department

Minnesota Mining and Manufacturing Company
425 13th Street NW
Washington, D.C.
Attn: Reynolds Marchant, Government Liaison
SNAP and Nuclear

Monsanto Research Corporation
Mound Laboratory
P.O. Box 32
Miamisburg, Ohio 45352
Attn: G. R. Grove

NASA
Langley Research Center
Langley Station
Hampton, Virginia 23365
Attn: Librarian

NASA
Goddard Space Flight Center
Glenn Dale Road
Greenbelt, Maryland 20771
Attn: Charles Baxter, Nimbus Project (1)
A. W. Fihelly, Nimbus Project (1)

NASA
Lewis Research Center
21000 Brookpark Road
Cleveland, Ohio 44135
Attn: George Mandel

NASA
George C. Marshall Space Flight Center
Huntsville, Alabama 35812
Attn: W. Y. Jordan

NASA
Ames Research Center
Moffet Field, California
Attn: Glenn Goodwin

NASA
Headquarters
1512 H Street NW
Washington, D.C. 20545
Attn: Thomas B. Kerr

NASA
Manned Spacecraft Center
Houston, Texas 77058
Attn: Chief, Technical Information Division

NASA
Scientific and Technical Information Facility
P.O. Box 5700
Bethesda, Maryland 20014
Attn: NASA Representative, S-AK/DL (2)

Nuclear Utility Services, Inc.
1730 M Street NW
Washington, D.C. 20036
Attn: Morton S. Goldman, Manager Environmental
Safeguards

Phillips Petroleum Company
NRTS Technical Library
P.O. Box 2067
Idaho Falls, Idaho 83401

Radio Corporation of America
Astroelectronics Division
Princeton, New Jersey

Director, USAF Project RAND
Via Air Force Liaison Office
The Rand Corporation
1700 Main Street
Santa Monica, California 90406
Attn: Library

TRW Systems
P.O. Box 287
Redondo Beach, California
Attn: Dr. Donald Jortner

U. S. Naval Radiological Defense Laboratory
Commanding Officer and Director
San Francisco, California 94135
Attn: Dr. P. E. Zigman

Union Carbide Research Institute
P.O. Box 278
Tarrytown, New York
Attn: Joseph Agresta, Space Sciences Group

Union Carbide Corporation
Nuclear Division
P.O. Box X
Oak Ridge, Tennessee 37831
Attn: E. Lamb, Isotope Devel. Ctr. (2)

University of California
Lawrence Radiation Laboratory
P.O. Box 808
Livermore, California 94551
Attn: Technical Information Division

Westinghouse Electric Company
Astronuclear Laboratory
P.O. Box 10864
Pittsburgh 30, Pennsylvania
Attn: Joanne M. Bridges
Supervisor Flight Safety Analysis Group

DISTRIBUTION (cont):
Aeronautical Systems Division
Wright-Patterson Air Force Base, Ohio 45433
Attn: Augustus Daniels, SEPRR

Division of Technical Information Ext.
USAEC
P.O. Box 62
Oak Ridge, Tennessee 37831 (70)

Clearinghouse for Federal Scientific and
Technical Information
5285 Port Royal Road
Springfield, Virginia 22151 (75)

General Electric Company
Nuclear Materials and Propulsion Operation
P.O. Box 15132
Cincinnati, Ohio 45212
Attn: J. W. Stephenson
For: W. Briskin

University of California
Lawrence Radiation Laboratory
P.O. Box 808
Livermore, California 94551
Attn: Dr. James Hadley
Chief, R Division

USAEC, SNPO
Westinghouse Electric Company
Astronuclear Laboratory
P.O. Box 10864
Pittsburgh 30, Pennsylvania
Attn: H. P. Smith

Institute for Defense Analysis
400 Army Navy Drive
Arlington, Virginia 22200
Attn: Richard Briceland

Mr. Norman Shartzer
Dept. of Atmospheric Science
SUNY at Albany
135 Western Avenue
Albany, New York 12203

The Travelers Research Center, Inc.
250 Constitution Plaza
Hartford, Connecticut 06103
Attn: K. D. Hage (12)

S. P. Schwartz, 1
R. W. Henderson, 1000
L. A. Hopkins, 1300
J. H. Findlay, 1400
S. A. Moore, 1540
R. J. Jansen, 4200
R. S. Claassen, 5100
J. R. Banister, 5120
T. B. Cook, 5200
J. D. Shreve, 5234
C. Winter, 5630
W. T. Moffat, 7220
V. E. Viney, 7250
L. E. Lamkin, 7300
G. H. Roth, 7320
G. A. Fowler, 9000
D. B. Shuster, 9200
A. E. Bentz, 9232
A. Y. Pope, 9300
V. E. Blake, 9310
H. E. Hansen, 9311 (3)
S. L. Jeffers, 9312 (2)
S. McAlees, 9314
J. D. Appel, 9319 (2)
R. C. Maydew, 9320
H. R. Vaughn, 9321
W. H. Curry, 9322
E. C. Rightley, 9323
W. H. Barton, 9324
K. J. Touryan, 9326
W. N. Caudle, 9327
W. N. Caudle, 9327
Attn: J. Colp
A. J. Clark, 9330
J. W. McKiernan, 9331
J. L. Tischhauser, 9420
B. S. Biggs, 8000
B. F. Hefley, 8232
B. R. Allen, 3421
M. G. Randle, 3428-1
R. S. Gillespie, 3413 (2)
C. Sproul, 3415-3 (10)